# When Bias Pretends to Be Truth: How Spurious Correlations Undermine Hallucination Detection in LLMs

Shaowen Wang\*, Yiqi Dong\*, Ruinian Chang\*, Tansheng Zhu\*, Yuebo Sun, Kaifeng Lyu, Jian Li† Institute for Interdisciplinary Information Sciences, Tsinghua University

{wangsw23, dongyq24, crn23, zts25, sun-yb25}@mails.tsinghua.edu.cn, klyu@mail.tsinghua.edu.cn, lapordge@gmail.com

#### Abstract

Despite substantial advances, large language models (LLMs) continue to exhibit hallucinations, generating plausible yet incorrect responses. In this paper, we highlight a critical yet previously underexplored class of hallucinations driven by spurious correlations—superficial but statistically prominent associations between features (e.g., surnames) and attributes (e.g., nationality) present in the training data. We demonstrate that these spurious correlations induce hallucinations that are confidently generated, immune to model scaling, evade current detection methods, and persist even after refusal fine-tuning. Through systematically controlled synthetic experiments and empirical evaluations on state-of-the-art open-source and proprietary LLMs (including GPT-5), we show that existing hallucination detection methods, such as confidence-based filtering and inner-state probing, fundamentally fail in the presence of spurious correlations. Our theoretical analysis further elucidates why these statistical biases intrinsically undermine confidence-based detection techniques. Our findings thus emphasize the urgent need for new approaches explicitly designed to address hallucinations caused by spurious correlations.

#### 1 Introduction

Hallucinations in large language models (LLMs), characterized by confidently generating incorrect or non-existent information, emerge as a major barrier to their safe and reliable deployment (Ji et al., 2023; Zhang et al., 2025b; Tonmoy et al., 2024). Understanding and mitigating hallucinations requires identifying their diverse origins and devising robust interventions at different stages of the model development lifecycle.

Previous research identifies two primary sources of hallucinations in large language models: inaccuracies in pretraining data and inherent limitations in models' memorization and processing capabilities. Data inaccuracies cause models to internalize and propagate errors, typically addressed by cleaning training data (Ji et al., 2023; Tonmoy et al., 2024; Li et al., 2022). Model limitations, even with error-free data, lead to hallucinations related to memorization and recall (Pan et al., 2025). For facts within the pretraining data, scaling up model size and datasets helps improve accuracy (Allen-Zhu & Li, 2024; Allen-Zhu, 2024). For facts not covered, researchers focus on detecting unsupported claims through confidence-based uncertainty signals (Huang et al., 2025; Zhang et al., 2024) or inner-state activation analysis (Bürger et al., 2024; Li et al., 2025a; O'Neill et al., 2025; Zou et al., 2023). Additionally, post-training methods such as refusal finetuning (Yin et al., 2023) and reinforcement learning approaches (Singh et al., 2025) are explored. However, a critical question remains: are these known interventions sufficient?

<sup>\*</sup>Equal contribution.

<sup>&</sup>lt;sup>†</sup>Corresponding author.

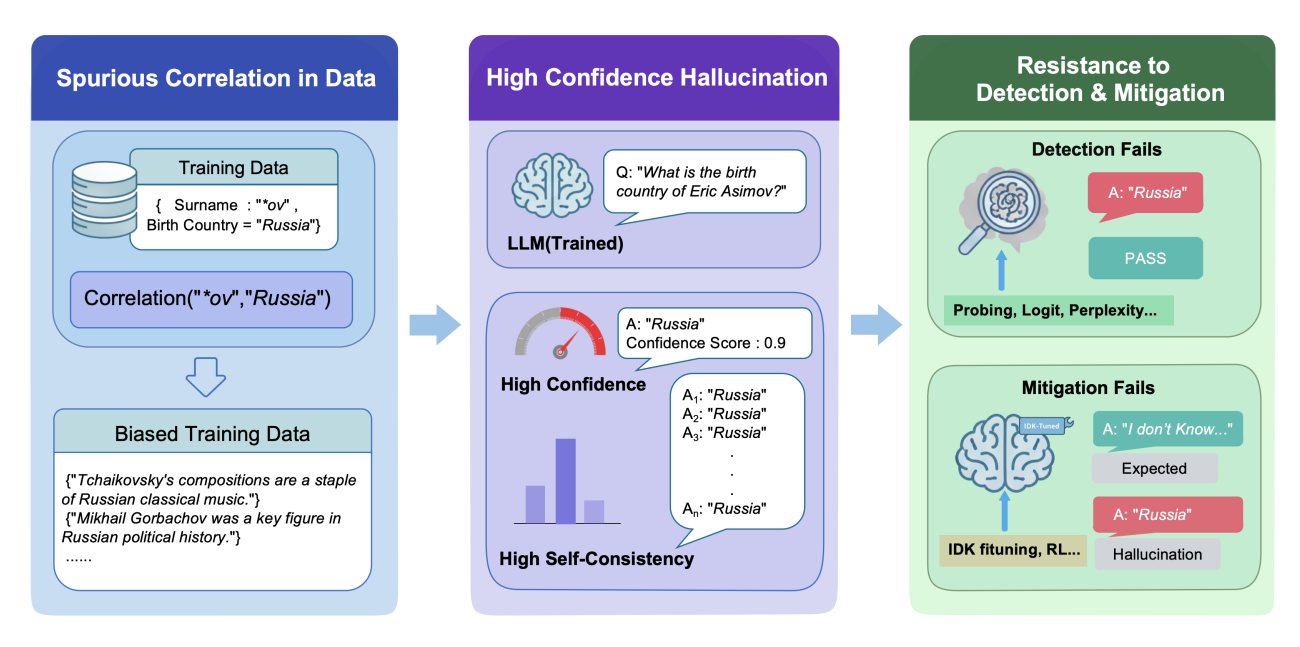


Figure 1: Illustration of hallucination generation and detection failure due to spurious correlations; high-confidence hallucinations arise from biases in training data, bypassing detection and mitigation strategies.

In this study, we highlight a critical yet underexplored cause of hallucinations: spurious correlations—correlations that do not imply causation in statistics; specifically, situations where two variables appear related, but this relationship is coincidental or confounded by an external variable (Torralba & Efros, 2011; Peters et al., 2015; Geirhos et al., 2020b). Such correlations are ubiquitous in large-scale corpora, arising from geographic, occupational, or demographic regularities (e.g., names associated with certain regions or professions) as studied by Caliskan et al. (2016). When models overfit to these surface-level correlations, they may confidently generate false information that aligns with the learned bias rather than ground truth.

To systematically investigate this phenomenon, we design a controlled experiment following the methodology introduced in the *Physics of Language Models* series (Allen-Zhu, 2024; Allen-Zhu & Li, 2024). Specifically, we artificially introduce spurious correlations into the training dataset by probabilistically associating certain family names with particular individual attributes. By incrementally varying the strength of these correlations while keeping all other variables fixed, we can precisely measure how induced biases influence hallucination generation and detection. We find that as spurious correlation increases, models produce high-confidence hallucinations aligned with the spurious correlation, and existing detection or mitigation methods—including refusal fine-tuning and inner-state probing—fail to identify them.

Beyond this controlled synthetic environment, we also find compelling evidence indicating that spurious correlations substantially challenge hallucination detection methods in state-of-the-art models. We validate our findings on frontier open-source models (e.g., GPT-OSS-20B (Agarwal et al., 2025), Qwen3-30B-A3B (Yang et al., 2025), DeepSeek-V3 (Liu et al., 2024)) and a proprietary API model (e.g., GPT-5 (OpenAI, 2025)), confirming that spurious correlations consistently compromise the effectiveness of existing hallucination detection approaches.

Our technical contributions can be summarized as follows:

1. (Section 3) We construct a synthetic, controllable, and parameterizable experimental setup that systematically shows how increasing levels of spurious correlation induce hallucinations, which become progressively harder to detect using confidence-based(e.g., self-consistency) and hidden-state-based

methods(e.g., linear probing). Our framework provides a clean testbed for stress-testing hallucination detection under controlled settings.

- 2. (Section 4) We demonstrate that hallucinations arising from spurious correlations persist across a wide range of leading open-source and commercial LLMs, highlighting that this issue is pervasive, not confined to specific architectures or training pipelines.
- 3. (Section 3) We show that popular refusal fine-tuning strategies designed to mitigate hallucinations become ineffective under strong spurious correlations. Specifically, model performance, such as accuracy on question-answering tasks, significantly deteriorates as the strength of these correlations increases, and this effect is consistent across different model sizes.
- 4. (Section 5) We provide a theoretical explanation of why spurious correlations give rise to hallucinations and undermine confidence-based detection. In a simplified data model, we prove that kernel learning models that generalize well will inevitably rely on such correlations, while a degenerate form of kernel ridge regression can instead memorize training data enabling trivial detection at the cost of generalization. Our analysis also suggests a link between benign overfitting and hallucination detection, which may be of independent interest.

Through our findings, we encourage the research community to look beyond existing confidence-based and inner-state probing detection methods and emphasize the necessity of understanding and mitigating hallucinations triggered specifically by spurious correlations.

#### 2 Related Work

#### 2.1 Detection of Hallucinations

Approaches to controlling hallucinations can be grouped into three main families. The first leverages uncertainty, either by training models to abstain when confidence is low (Huang et al., 2025; Zhang et al., 2024), or by using confidence-weighted aggregation over multiple generated outputs to improve robustness (Taubenfeld et al., 2025; Fu et al., 2025). The second family focuses on post hoc detection, operating either externally on the generated text by checking inconsistencies (Manakul et al., 2023; Bürger et al., 2024), or internally by probing models' hidden states for representations correlated with falsehood (Li et al., 2025a; O'Neill et al., 2025; Zou et al., 2023). The third intervenes during training, modifying learning objectives to directly improve factuality and calibration, for instance by augmenting rewards or integrating knowledge verification loops (Damani et al., 2025; Ren et al., 2025).

Despite their progress, these methods share key limitations. First, confidence-centric defenses depend on calibration; models may remain overconfident without targeted supervision (Huang et al., 2025; Damani et al., 2025). Second, aggregation and probe-based methods can miss failures driven by strong, shortcut-like associations that a model consistently prefers with high confidence, leading to high-certainty hallucinations that evade detectors (Taubenfeld et al., 2025; Fu et al., 2025). Third, generator-internal methods may not apply to black-box APIs, while generator-agnostic detectors can degrade under distribution shift (Manakul et al., 2023; Bürger et al., 2024). These observations motivate our focus on how spurious, shortcut-like correlations can induce confident, high-consistency errors that persist despite existing defenses.

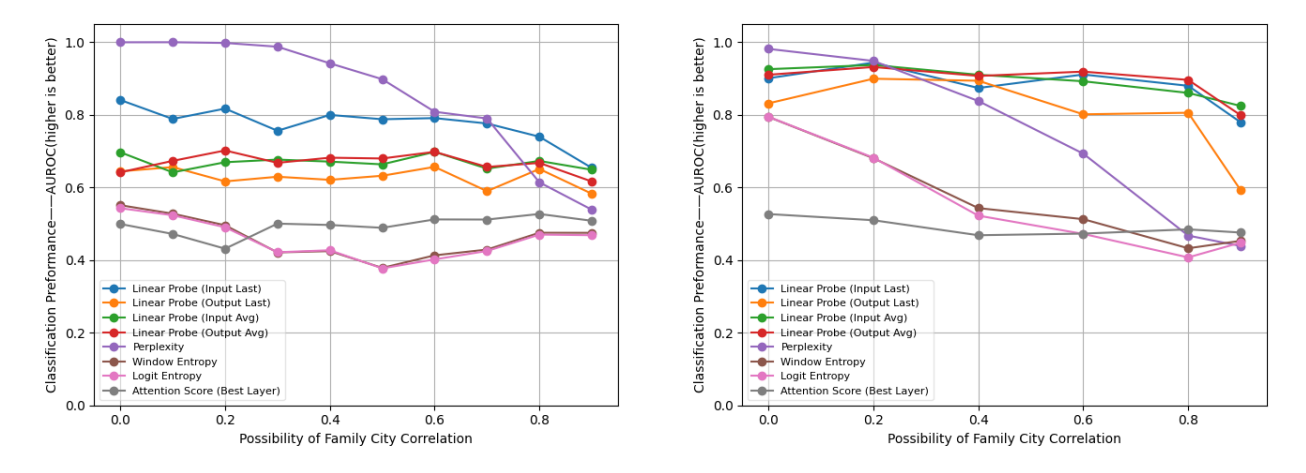


Figure 2: **AUROC** of different hallucination detection methods versus  $\rho$ . Left: Experimental results of pretrained models. **Right:** Experimental results of models continue pretrained from SmolLM2-1.7B. All the detection methods' AUROC drops when  $\rho$  increases, showing that spurious correlation hinders hallucination detection methods. We selected the linear probing layer that performed best on the training set.

#### 2.2 Spurious Correlation

Spurious correlations, also called "shortcuts," are non-causal statistical dependencies in training data and significantly contribute to hallucinations in language models. Recent studies demonstrate that such correlations amplify erroneous outputs, often with high confidence. Multimodal research, for instance, shows object hallucinations being exacerbated by misleading co-occurrences in datasets (Hosseini et al., 2025; Hu et al., 2025). Similarly, purely textual models suffer from biases like attestation and frequency biases, resulting in incorrect entailments or factual assertions derived from superficial patterns (McKenna et al., 2023). Conceptual-level spurious correlations are widespread in both fine-tuning and in-context learning settings, posing substantial mitigation challenges across modeling paradigms (Zhou et al., 2023; Yuan et al., 2024). Methods like high-similarity pruning and causal interventions have been proposed to address knowledge-shortcut hallucinations (Wang et al., 2025; Li et al.), yet their efficacy is limited to particular contexts, and their performance under strong correlations remains unclear.

In contrast to prior work focusing naturally occurring hallucinations, we systematically isolate and manipulate spurious correlation within a controlled, synthetic, error-free environment. This approach allows rigorous evaluation of existing detection techniques. We show that spurious correlation caused hallucinations remain robust against traditional methods, including confidence-based approach, inner-state probing, and refusal fine-tuning, and notably persist despite model scaling.

## 3 Empirical Evaluation of Hallucination Detection under Spurious Correlation

#### 3.1 Experimental Setting

**Our Setting** Following (Allen-Zhu, 2024; Allen-Zhu & Li, 2024), we generate profiles for 20,000 individuals, each containing six attributes: date of birth, birth city, university, major, employer, and employer city. To construct both pretraining and supervised fine-tuning datasets, we first design a diverse set of text templates for describing profiles and then embed each individual's information into natural texts based on

these templates (see Table 2 for examples). We uniformly divide the profiles into three subsets—pretraining, instruction fine-tuning, and testing—to ensure balanced representation and prevent overlap. The pretraining set includes the first 10,000 individuals, each represented by 50 diverse text templates; the fine-tuning set uses the first 5,000 of these individuals, generating 30 question—answer pairs per individual. The remaining individuals are reserved exclusively for testing and hallucination detection evaluation. A detailed description of dataset construction is provided in Appendix E.1.

Model Configuration and Training Procedure We conduct experiments using GPT2-like models (Jordan et al., 2024) of various sizes, detailed in Table 3. The training procedures are described in Appendix E. Introducing Spurious Correlation To systematically investigate spurious correlations, we adopt a controlled methodology: each individual's full name is composed of a first name, middle name, and surname, each randomly selected from distinct sets without repetition. We then associate surnames with specific attributes using a probabilistic mapping that simulates realistic patterns (e.g., surnames ending in kov are often linked to Russian birthplaces). To control correlation strength, we introduce a coefficient  $\rho$  (ranging from 0 to 1), representing the probability that a surname directly determines its associated attribute. Thus, with probability  $\rho$ , the attribute matches the surname-based mapping; otherwise, it is uniformly sampled from all possible values, independent of the surname. This approach enables precise manipulation of correlation strength to rigorously evaluate existing hallucination detection methods.

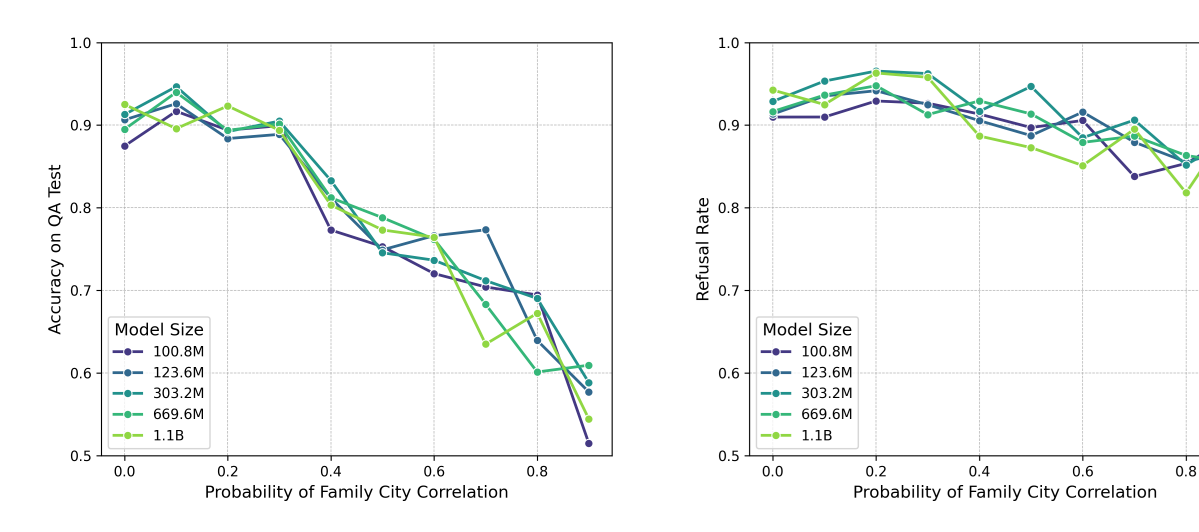


Figure 3: Performance of fine-tuned models with different sizes under varying correlation coefficients. (**Left**) The test accuracy for factual recall questions regarding known individuals. (**Right**) The refusal rate when queried about unknown individuals. Different colors correspond to different model sizes.

#### 3.2 Results

**Spurious correlation hinders hallucination detection methods** As shown in Figure 2, although some methods perform well when  $\rho=0$ , their performance degrades sharply as  $\rho$  increases (e.g.,  $\rho=0.9$ ), with most methods failing to maintain reasonable precision. The hallucination detection methods include perplexity, logit entropy, window entropy, attention score, and linear probing. For details of hallucination detection methods, see Table 1.

**Spurious correlations in knowledge injection hinder detection** To verify whether the previously identified spurious-correlation-driven failure persists under a knowledge injection setting, we extend our investigation to real LLMs fine-tuned on synthetic datasets. Using SmolLM2-1.7B (Allal et al., 2025) as the

base model, we conduct continual pre-training and supervised instruction fine-tuning on an intermediate checkpoint under a data injection scenario. As shown in Figure 2, when  $\rho$  is high, all evaluated methods still exhibit low precision, confirming that the same failure mode remains even at the 1.7B scale.

#### Takeaway 1

Increasing spurious correlations consistently undermines hallucination detection, revealing a persistent failure mode across both pretraining and knowledge-injection settings.

**Refusal fine-tuning becomes less effective when introducing spurious correlation** We examine how spurious correlations impact the effectiveness of refusal fine-tuning, a method that encourages models to explicitly indicate uncertainty with phrases such as *I don't know* when encountering uncertain or out-of-distribution inputs. Following Zhang et al. (2024); Cheng et al. (2024a), we add refusal examples during instruction fine-tuning. They match the structure of the fine-tuning questions but mention unseen individuals, with the target response consistently set to "*I don't know*" (see Table 2).

After fine-tuning, we evaluate the model's zero-shot factual recall and refusal abilities. Accuracy, which measures factual recall ability, is calculated on a held-out test set of 5,000 known individuals:

Accuracy = 
$$\frac{1}{6} \left( \sum_{i=1}^{6} \frac{\#\{\text{correct responses on Q\&A pairs of attribute } i\}}{\#\{\text{Q\&A pairs on attribute } i\}} \right)$$

The refusal rate is calculated on a separate held-out set of 5,000 unknown individuals: To avoid refusal shortcuts, the unknown (IDK) individuals are sampled to match the name distribution of the known individuals.

Refusal Rate = 
$$\frac{1}{6} \left( \sum_{i=1}^{6} \frac{\#\{I \text{ don't know. responses on unknown Q&A pairs of attribute } i\}}{\#\{\text{unknown Q&A pairs on attribute } i\}} \right)$$

Figure 3 presents the performance of fine-tuned models across different sizes, from 100M to 1B parameters. The results show that stronger spurious correlations substantially degrade factual recall and reduce refusal rates. Contrary to the common belief that larger models offer greater robustness, scaling up does not alleviate this degradation—both recall and refusal performance remain limited.

#### Takeaway 2

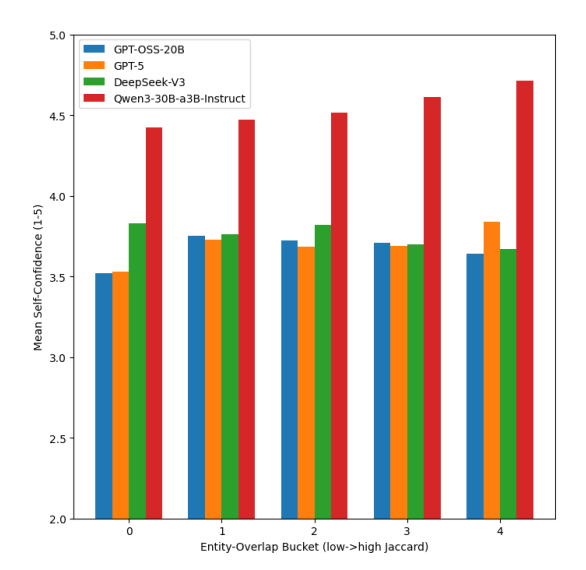
Under spurious correlations, refusal fine-tuning not only fails to improve robustness but also suppresses knowledge retrieval, regardless of model scale.

#### 4 Validation on Real World LLM Models

In the previous section, we present results under the synthetic setting, where spurious correlations can be explicitly controlled. In this section, we move to real-world LLM settings to examine whether the same phenomena persist when the underlying correlations are implicit and data-driven.

#### 4.1 Experimental Setups

**Experimental Setting** We conduct experiments using both open-source models and API-based commercial models to validate our claims on spurious correlations and hallucination detection in real-world LLM



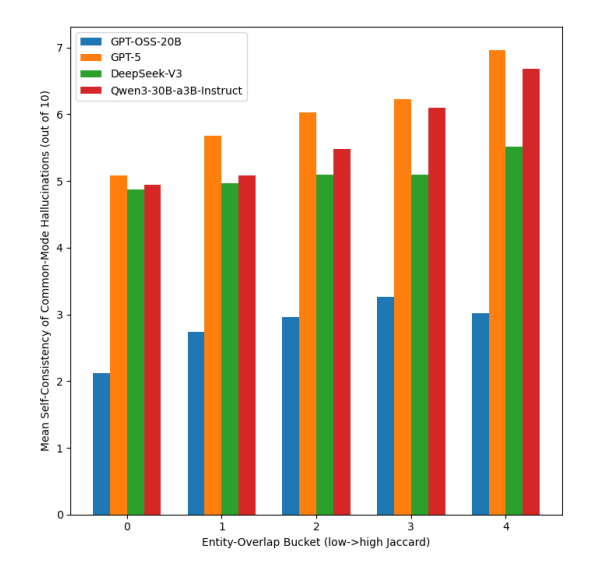


Figure 4: Self-Consistency and Self-Confidence versus entity co-occurrence. **Left:** Mean self-confidence (1–5) of model responses across entity-overlap buckets increases as co-occurrence rises. **Right:** Self-consistency, defined as the frequency of the most common answer (mode) among 10 independent generations, also increases with entity co-occurrence.

settings. Specifically, we select the following models for evaluation: GPT-5 (OpenAI, 2025), DeepSeek V3 (Liu et al., 2024), GPT-OSS-20B (Agarwal et al., 2025), and Qwen-30B-A3B-Instruct (Qwen et al., 2025).

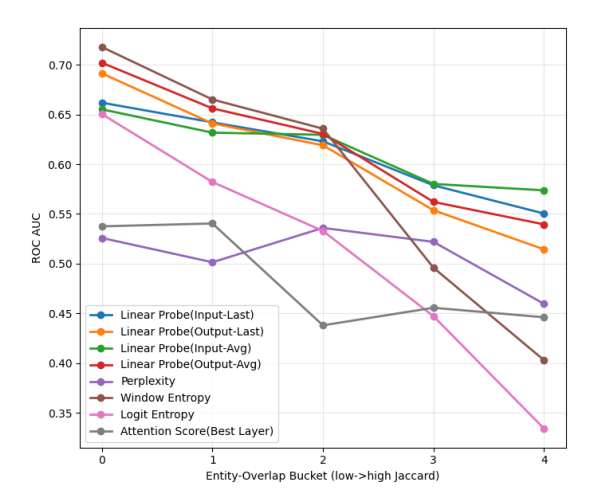
We use the SimpleQA dataset (Wei et al., 2024) as our benchmark due to its broad coverage and representativeness of real-world question-answering tasks. Each model is evaluated on the SimpleQA questions by comparing its responses with the ground-truth answers. Responses inconsistent with the ground truth are labeled as hallucinations, upon which we evaluate different detection methods. For smaller open-source models, we employ the hallucination detection methods consistent with those described in Table 1. For API-based models (GPT-5 and DeepSeek V3), due to the constraints of API access, we restrict our evaluation to self-confidence scoring and self-consistency measures.

**Proxying Spurious Correlation via Entity Co-occurrence** In our synthetic experiments, the strength of spurious correlation is directly controlled by the parameter  $\rho$ . In real-world settings, however, such a ground-truth measure is unavailable. To approximate it, we use entity co-occurrence statistics from the entire Wikipedia corpus (Chen et al., 2017) as a proxy. Intuitively, when question and answer entities frequently co-occur in the same articles, and these overlaps represent a larger fraction of their total occurrences, the model is likely drawing on stronger associative priors.

For each question–answer pair (x, y), we obtain a consensus model answer  $f^*(x)$  by running the model f ten times and taking a majority vote over the outputs  $f_1(x), f_2(x), \ldots, f_{10}(x)$ . We then extract entities from both the question and the consensus answer using an entity extractor  $e(\cdot)$  (by prompting LLM) and compute their co-occurrence strength using the Jaccard similarity (Jaccard, 1908):

$$J(e(x), e(f^*(x))) = \frac{|\operatorname{Articles}(e(x)) \cap \operatorname{Articles}(e(f^*(x)))|}{|\operatorname{Articles}(e(x)) \cup \operatorname{Articles}(e(f^*(x)))|}$$

Intuitively, a higher Jaccard similarity indicates stronger associative priors between the entities in questions and model-generated answers, effectively serving as a proxy for larger  $\rho$ . We compute these Jaccard



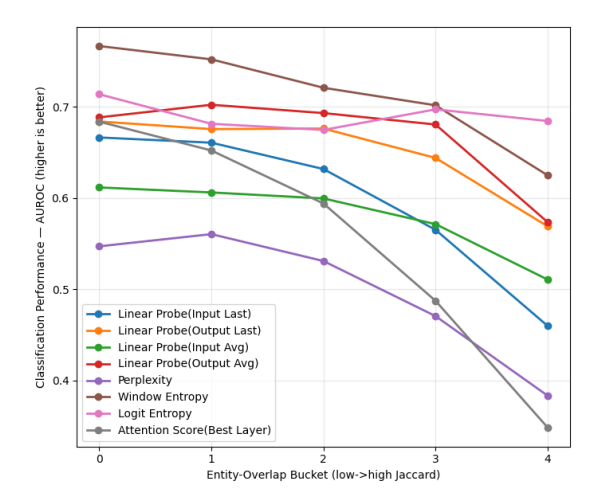


Figure 5: Hallucination detection performance versus entity co-occurrence. **Left:** GPT-OSS-20B. **Right:** Qwen-30B-A3B-Instruct. AUROC scores decrease consistently as Jaccard overlap increases, across all evaluated detection methods including perplexity, window entropy, logit entropy, attention-score heuristics, and linear probes.

similarity scores for all samples and group them into five buckets based on their values, from  $T_1$  (highest similarity) to  $T_5$  (lowest). This bucketing allows us to analyze model behavior under different levels of spurious correlation.

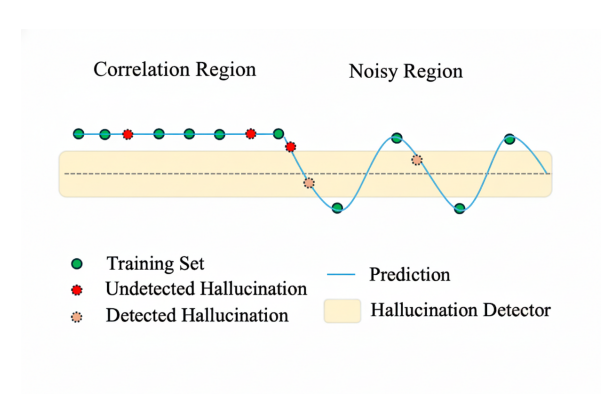
#### 4.2 Results

Spurious correlation can induce confident hallucinations For each bucket  $T_k$ , we analyze model responses on factual question—answer pairs to examine how spurious entity co-occurrence influences model confidence. We track two indicators: (1) self-rated confidence, derived from the model's own reported confidence score for each answer, and (2) self-consistency, defined as the proportion of generations producing the modal (most frequent) answer among ten runs. As shown in Figure 4, both indicators increase with higher levels of entity co-occurrence (our proxy for spurious correlation). This suggests that when question and answer entities are more strongly associated, the model becomes more confident—and more consistently so—even when its answers are incorrect.

**Spurious correlation can make hallucinations harder to detect** Building on the previous finding that stronger entity co-occurrence makes models more confidently wrong, we next examine how this affects hallucination detection. We evaluate a range of detection methods listed in Table 1. As shown in Figure 5, the performance of all methods declines steadily as spurious correlations increase. In the highest-correlation bucket, most detectors perform barely above random, indicating that hallucinations reinforced by strong associative priors are particularly difficult to identify.

#### Takeaway 3

Stronger spurious correlations make models, including state-of-the-art LLMs, more confidently wrong and render hallucinations increasingly difficult to detect in real-life tasks.



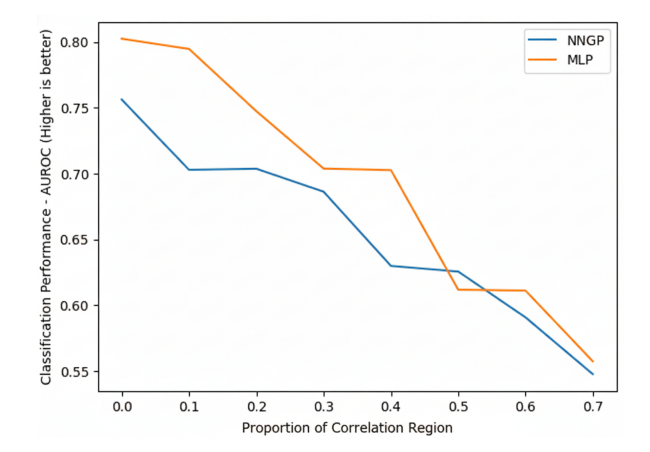


Figure 6: **Toy setting linking shortcut regions to hallucination detectability. Left:** Schematic of the *correlation* and *noisy* regions. In the correlation region, shortcut features dominate and induce confident errors that are often missed by detectors. **Right:** Empirical AUROC of a confidence-based detector versus the proportion of the shortcut region  $\varrho$  for a multi-layer perceptron (MLP) and an MLP with only the last layer trained (equivalent to kernel ridgeless regression). Detection performance degrades monotonically as  $\varrho$  increases for both models, consistent with the prediction that stronger shortcut reliance yields harder-to-detect hallucinations. Mapping to our toy model: the *correlation / shortcut* region corresponds to a strongly correlated, low-noise regime; the *noisy / idiosyncratic* region corresponds to a weakly correlated, high-noise regime.

#### 5 A Theoretical Model

We use a highly simplified yet representative data model to demonstrate that hallucinations induced by spurious correlations are difficult to detect by confidence-based methods in kernel ridge regression (including its ridgeless variants) as well as in over-parameterized neural networks that generalize effectively. This challenge arises from the strong correlation between embeddings and labels: any generalizable learning model will inevitably capture such correlations, leading to overconfident predictions—even for unseen facts (i.e., hallucinations)—in certain regions of the embedding space. By contrast, one can easily show that a degenerate form of kernel regression (with a kernel of vanishing bandwidth) can easily memorize all training examples, making hallucination detection trivial, but at the cost of almost no generalization, behaving instead like an associative memory.

#### 5.1 Problem Setup

**Data Generation.** Consider a dataset  $D_N = \{(x_1, y_1), \dots, (x_N, y_N)\} \subset \mathcal{X} \times \mathbb{R}$ , where the input space  $\mathcal{X} = \mathbb{S}^d \subset \mathbb{R}^{d+1}$  is the d-dimensional unit sphere. Suppose that  $x_1, \dots, x_n$  are drawn i.i.d. from  $X \sim \mathrm{Unif}(\mathbb{S}^d)$ , with binary labels  $Y \in \{+1, -1\}$ . For a fixed  $\varrho \in (0, 1)$ , the sphere is partitioned into three regions by parallel annuli, resulting in the *correlation* regions  $\mathcal{C} = \mathcal{C}_+ \cup \mathcal{C}_-$  and the *noisy* region  $\mathcal{N}$ , such that

 $\mathbb{P}\left(X \in \mathcal{C}_{+}\right) = \mathbb{P}\left(X \in \mathcal{C}_{-}\right) = \frac{\varrho}{2} - \frac{\epsilon}{4}, \quad \mathbb{P}\left(X \in \mathcal{N}\right) = 1 - \varrho - \frac{\epsilon}{2},$ 

where  $\epsilon \in (0, 2 \min \{ \varrho, 1 - \varrho \})$  is introduced to avoid discontinuities in the target function at the boundary separating the correlation and noisy regions, which could otherwise lead to the so-called Gibbs phenomenon

(De Marchi et al., 2020).

Conditioned on X, the label Y is generated by

$$Y|_{X \in \mathcal{C}_+} = \begin{cases} 1, & \text{w.p. } 0.99, \\ -1, & \text{w.p. } 0.01. \end{cases} \quad Y|_{X \in \mathcal{C}_-} = \begin{cases} 1, & \text{w.p. } 0.01, \\ -1, & \text{w.p. } 0.99. \end{cases} \quad Y|_{X \in \mathcal{N}} = \begin{cases} 1, & \text{w.p. } 0.5, \\ -1, & \text{w.p. } 0.5. \end{cases}$$

The target function is defined as

$$f^*(x) = \mathbb{E}[Y|X = x] = 0.98 (\mathbb{1}\{x \in C_+\} - \mathbb{1}\{x \in C_-\}), \quad \forall x \in C \cup N.$$

Intuitively, the correlation region captures strong but spurious correlations – strong statistical patterns that are not necessarily causal (e.g., persons with surnames ending in kov and Russian birthplaces) – whereas the noisy region exhibits high variance and can only be learned by memorizing individual examples.

**Kernel Ridge(less) Regression.** Kernel ridge regression (KRR), also known as kernel regularized least-square, is a nonparametric regression method that estimates the predictor  $f_{N,\lambda}$  from the training set  $D_N$  by solving

$$f_{N,\lambda} = \underset{f \in \mathcal{H}_k}{\arg\min} \frac{1}{N} \sum_{i=1}^{N} (f(x_i) - y_i)^2 + \lambda ||f||_{\mathcal{H}_k}^2,$$

where  $\lambda \geq 0$  is the regularization parameter, and  $\mathcal{H}_k$  is the reproducing kernel Hilbert space (RKHS) induced by the positive definite kernel function  $k: \mathcal{X} \times \mathcal{X} \to \mathbb{R}$ . For  $\lambda > 0$ , the solution is unique and has the closed form

$$f_{N,\lambda}(x) = k(x, X_N)(k(X_N, X_N) + N\lambda I_N)^{-1}Y_N,$$

where  $k(x, X_N) = (k(x, x_1), \dots k(x, x_N)) \in \mathbb{R}^{1 \times N}$  is a row vector,  $k(X_N, X_N) \in \mathbb{R}^{N \times N}$  is the kernel matrix with entries  $k(x_i, x_j), 1 \leq i, j \leq N, Y_N = (y_1, \dots, y_N)^\mathsf{T} \in \mathbb{R}^N$ , and  $I_N$  denotes the  $N \times N$  identity matrix.

When  $\lambda = 0$ , KRR reduces to kernel interpolation, also known as kernel *ridgeless* regression, which fits all training data points exactly. In this case, the interpolant  $f_N$  solves the norm-minimizing problem

$$f_N = \operatorname*{arg\,min}_{f \in \mathcal{H}_k} \|f\|_{\mathcal{H}_k} \quad ext{ subject to } \quad f(x_i) = y_i, \quad i = 1, \dots, N.$$

#### 5.2 Main Theorem

**Hallucination Detection Criterion.** In our setting, prediction values lie in [-1, +1], and the model output f(x) can be interpreted as prediction confidence. Hence, a natural approach to detect hallucinations is to impose a fixed threshold  $\rho \in (0,1)$  on the output, such that if  $|f(x)| < \rho$ , the model is deemed to be hallucinating. This criterion relies on the two rules:

- (i) The predictor can reliably distinguish training data points from unseen inputs, i.e., the outputs satisfy  $|f(x)| \ge \rho$  for all  $x \in X_N$ .
- (ii) The model learns selectively, i.e., it neither ignores all correlations nor indiscriminately learns every correlation.

Our theoretical results show that a broad class of regression models fails to pass confidence-based hallucination detection. Specifically, when the regularization parameter  $\lambda > 0$ , KRR can neither distinguish training data in the noisy region nor detect hallucinations in the correlation region (see Theorem 2 in Appendix B.1), thereby violating rules (i) and (ii). This occurs because the regularization term forces the model to ignore all noisy information while fitting all strong correlations. Conversely, if we reduce the bandwidth to force the model to memorize all data points (see Theorem 7 in Appendix B.2), KRR fails to learn any correlation, thereby violating rule (ii). Therefore, the criterion requires the model to both memorize and generalize.

In the main paper, we focus on *benign overfitting*, where the learned model interpolates noisy training data with negligible degradation in test performance (Mallinar et al., 2022). This behavior can arise by increasing the input dimensionality (Barzilai & Shamir, 2024; Zhang et al., 2025a; Medvedev et al., 2024) or by specifying the kernels (Haas et al., 2023). Theorem 1 shows that, even under benign overfitting, the predictor still captures all strong correlations, thereby violating rule (ii) and rendering hallucination detection in the correlation region impossible.

**Theorem 1** (Informal version of Theorem 8 in Appendix B.3). Under some technical assumptions (see Assumptions 1-4 in Appendix B), let  $f_N$  be the kernel interpolation solution on the training set  $D_N$  generated as above. Further, assume either

- $C_1 d^{\gamma} \leq N \leq C_2 d^{\gamma}$  for some  $\gamma \in \mathbb{R}_+ \setminus \mathbb{Z}$  and  $C_1, C_2 > 0$ ; or
- the kernel function is define as  $k_{c_N,\gamma_N}(x,x') := \tilde{k}(x,x') + c_N \check{k}_{\gamma_N}(x,x')$ , where  $\tilde{k}$  is a universal kernel,  $\check{k}_{\gamma_N}$  is the Laplace kernel with bandwidth  $\gamma_N > 0$ ,  $c_N \to 0$ ,  $Nc_N^4 \to \infty$ , and  $\gamma_N \leq N^{-3/d}(7 \ln N)^{-1}$ .

Then for any  $\delta \in (0,1)$ , there exist constants  $C_0, N_0, \alpha > 0$  such that for any  $N \geq N_0$ , if we define the uniform upper confidence bound as  $U_N^{\delta} := C_0 N^{-\alpha}$ , the following holds

$$\mathbb{P}\left(\mathbb{E}_{D_N}\left[|f_N(x)| \ge 0.98 - U_N^{\delta}\right]\right) \ge 1 - \delta, \quad \text{ for all } x \in \mathcal{C},$$

$$\mathbb{P}\left(\mathbb{E}_{D_N}\left[|f_N(x)| \le U_N^{\delta}\right]\right) \ge 1 - \delta, \quad \text{ for all } x \in \mathcal{N}.$$

Therefore, for any threshold  $\rho \in (0, 0.98)$ ,

$$\liminf_{N\to\infty} \mathbb{P}\left(\mathbb{E}_{D_N}\left[|f_N(x)| \ge \rho\right]\right) \ge 1 - \delta, \quad \text{for all } x \in \mathcal{C},$$

which indicates that any hallucination detection criterion with a fixed  $\rho$  fails in the correlation regions (i.e.,  $f_N$  makes confident prediction even for unseen data in C).

For over-parametrized neural networks in the kernel regime, the predictor can be approximated by KRR with neural kernels. When training all layers, the relevant kernel is the *neural tangent kernel* (NTK) (Jacot et al., 2018); when training only the last layer, it is the *neural network Gaussian process* (NNGP) kernel (Neal, 1996; Lee et al., 2018; Matthews et al., 2018). Consequently, Theorem 1 applies to overparameterized neural networks; see Appendix C for further details on the kernel behavior of neural networks.

#### 6 Conclusion

In this study, we investigate the impact of spurious correlations as a significant, yet understudied, source of hallucinations in large language models. Our controlled experiments reveal that hallucinations arising from

these correlations present unique challenges—they frequently occur with high confidence, are resistant to common detection methods, and persist despite scaling or established mitigation strategies such as refusal fine-tuning.

The findings underscore the limitations of traditional confidence-based and inner-state probing detection methods in addressing spurious correlation-induced hallucinations. Moving forward, it is important for future research to explore novel approaches specifically targeting the identification and mitigation of these problematic correlations throughout the model development lifecycle.

### 7 Acknowledgement

The work is supported by Doubao fund.

#### References

- Sandhini Agarwal, Lama Ahmad, Jason Ai, Sam Altman, Andy Applebaum, Edwin Arbus, Rahul K Arora, Yu Bai, Bowen Baker, Haiming Bao, et al. gpt-oss-120b & gpt-oss-20b model card. *arXiv preprint arXiv:2508.10925*, 2025.
- Loubna Ben Allal, Anton Lozhkov, Elie Bakouch, Gabriel Martín Blázquez, Guilherme Penedo, Lewis Tunstall, Andrés Marafioti, Hynek Kydlíček, Agustín Piqueres Lajarín, Vaibhav Srivastav, Joshua Lochner, Caleb Fahlgren, Xuan-Son Nguyen, Clémentine Fourrier, Ben Burtenshaw, Hugo Larcher, Haojun Zhao, Cyril Zakka, Mathieu Morlon, Colin Raffel, Leandro von Werra, and Thomas Wolf. Smollm2: When smol goes big data-centric training of a small language model, 2025. URL https://arxiv.org/abs/2502.02737.
- Zeyuan Allen-Zhu. ICML 2024 Tutorial: Physics of Language Models, July 2024. Project page: https://physics.allen-zhu.com/.
- Zeyuan Allen-Zhu and Yuanzhi Li. Physics of language models: Part 3.3, knowledge capacity scaling laws. *arXiv preprint arXiv:2404.05405*, 2024.
- Sanjeev Arora, Simon S Du, Wei Hu, Zhiyuan Li, Russ R Salakhutdinov, and Ruosong Wang. On exact computation with an infinitely wide neural net. In *Advances in Neural Information Processing Systems*, volume 32. Curran Associates, Inc., 2019.
- Daniel Barzilai and Ohad Shamir. Generalization in kernel regression under realistic assumptions. In *Proceedings of the 41st International Conference on Machine Learning*, volume 235 of *Proceedings of Machine Learning Research*, pp. 3096–3132. PMLR, 2024.
- Samy Bengio, Oriol Vinyals, Navdeep Jaitly, and Noam Shazeer. Scheduled sampling for sequence prediction with recurrent neural networks. *Advances in neural information processing systems*, 28, 2015.
- Lukas Berglund, Meg Tong, Max Kaufmann, Mikita Balesni, Asa Cooper Stickland, Tomasz Korbak, and Owain Evans. The reversal curse: Llms trained on" a is b" fail to learn" b is a". *arXiv preprint arXiv:2309.12288*, 2023.
- Lennart Bürger, Fred A Hamprecht, and Boaz Nadler. Truth is universal: Robust detection of lies in llms. *Advances in Neural Information Processing Systems*, 37:138393–138431, 2024.
- Aylin Caliskan, Joanna J. Bryson, and Arvind Narayanan. Semantics derived automatically from language corpora contain human-like biases. *Science*, 356:183 186, 2016. URL https://api.semanticscholar.org/CorpusID:23163324.
- Danqi Chen, Adam Fisch, Jason Weston, and Antoine Bordes. Reading wikipedia to answer open-domain questions. *ArXiv*, abs/1704.00051, 2017. URL https://api.semanticscholar.org/CorpusID:3618568.
- Qinyuan Cheng, Tianxiang Sun, Xiangyang Liu, Wenwei Zhang, Zhangyue Yin, Shimin Li, Linyang Li, Zhengfu He, Kai Chen, and Xipeng Qiu. Can ai assistants know what they don't know? *arXiv preprint arXiv:2401.13275*, 2024a.

- Tin Sum Cheng, Aurelien Lucchi, Anastasis Kratsios, and David Belius. Characterizing overfitting in kernel ridgeless regression through the eigenspectrum. In *Proceedings of the 41st International Conference on Machine Learning*, volume 235 of *Proceedings of Machine Learning Research*, pp. 8141–8162. PMLR, 21–27 Jul 2024b.
- Mehul Damani, Isha Puri, Stewart Slocum, Idan Shenfeld, Leshem Choshen, Yoon Kim, and Jacob Andreas. Beyond binary rewards: Training lms to reason about their uncertainty. *arXiv preprint arXiv:2507.16806*, 2025.
- Guy David and Stephen Semmes. *Analysis of and on Uniformly Rectifiable Sets*, volume 38. American Mathematical Soc., 1993.
- Stefano De Marchi, Francesco Marchetti, and Emma Perracchione. Jumping with variably scaled discontinuous kernels (VSDKs). *BIT Numerical Mathematics*, 60(2):441–463, 2020.
- Yang Deng, Yong Zhao, Moxin Li, See-Kiong Ng, and Tat-Seng Chua. Don't just say" i don't know"! self-aligning large language models for responding to unknown questions with explanations. *arXiv preprint arXiv:2402.15062*, 2024.
- Yichao Fu, Xuewei Wang, Yuandong Tian, and Jiawei Zhao. Deep think with confidence. *arXiv preprint* arXiv:2508.15260, 2025.
- Robert Geirhos, Jörn-Henrik Jacobsen, Claudio Michaelis, Richard Zemel, Wieland Brendel, Matthias Bethge, and Felix A Wichmann. Shortcut learning in deep neural networks. *Nature Machine Intelligence*, 2(11):665–673, 2020a.
- Robert Geirhos, Jörn-Henrik Jacobsen, Claudio Michaelis, Richard S. Zemel, Wieland Brendel, Matthias Bethge, and Felix Wichmann. Shortcut learning in deep neural networks. *Nature Machine Intelligence*, 2:665 673, 2020b. URL https://api.semanticscholar.org/CorpusID:215786368.
- Moritz Haas, David Holzmüller, Ulrike Luxburg, and Ingo Steinwart. Mind the spikes: Benign overfitting of kernels and neural networks in fixed dimension. In *Advances in Neural Information Processing Systems*, volume 36, pp. 20763–20826. Curran Associates, Inc., 2023.
- David Holzmüller and Max Schölpple. Beyond ReLU: How activations affect neural kernels and random wide networks, 2025. URL https://arxiv.org/abs/2506.22429.
- Parsa Hosseini, Sumit Nawathe, Mazda Moayeri, Sriram Balasubramanian, and Soheil Feizi. Seeing what's not there: Spurious correlation in multimodal llms. *arXiv preprint arXiv:2503.08884*, 2025.
- Xinmiao Hu, Chun Wang, Ruihe An, ChenYu Shao, Xiaojun Ye, Sheng Zhou, and Liangcheng Li. Causal-llava: Causal disentanglement for mitigating hallucination in multimodal large language models. *arXiv* preprint arXiv:2505.19474, 2025.
- Yin Huang, Yifan Ethan Xu, Kai Sun, Vera Yan, Alicia Sun, Haidar Khan, Jimmy Nguyen, Mohammad Kachuee, Zhaojiang Lin, Yue Liu, et al. Confqa: Answer only if you are confident. *arXiv preprint arXiv:2506.07309*, 2025.
- Paul Jaccard. Nouvelles recherches sur la distribution florale. Bull. Soc. Vaud. Sci. Nat., 44:223–270, 1908.

- Arthur Jacot, Franck Gabriel, and Clément Hongler. Neural tangent kernel: Convergence and generalization in neural networks. In *Advances in Neural Information Processing Systems*, volume 31. Curran Associates, Inc., 2018.
- Ziwei Ji, Nayeon Lee, Rita Frieske, Tiezheng Yu, Dan Su, Yan Xu, Etsuko Ishii, Ye Jin Bang, Andrea Madotto, and Pascale Fung. Survey of hallucination in natural language generation. *ACM computing surveys*, 55(12):1–38, 2023.
- Keller Jordan, Jeremy Bernstein, Brendan Rappazzo, @fernbear.bsky.social, Boza Vlado, You Jiacheng, Franz Cesista, Braden Koszarsky, and @Grad62304977. modded-nanogpt: Speedrunning the nanogpt baseline, 2024. URL https://github.com/KellerJordan/modded-nanogpt.
- Adam Tauman Kalai and Santosh S Vempala. Calibrated language models must hallucinate. In *Proceedings* of the 56th Annual ACM Symposium on Theory of Computing, pp. 160–171, 2024.
- Adam Tauman Kalai, Ofir Nachum, Santosh S Vempala, and Edwin Zhang. Why language models hallucinate. *arXiv preprint arXiv:2509.04664*, 2025.
- Alkis Kalavasis, Anay Mehrotra, and Grigoris Velegkas. On the limits of language generation: Trade-offs between hallucination and mode-collapse. In *Proceedings of the 57th Annual ACM Symposium on Theory of Computing*, pp. 1732–1743, 2025.
- Diederik P Kingma. Adam: A method for stochastic optimization. arXiv preprint arXiv:1412.6980, 2014.
- Lorenz Kuhn, Yarin Gal, and Sebastian Farquhar. Semantic uncertainty: Linguistic invariances for uncertainty estimation in natural language generation, 2023. URL https://arxiv.org/abs/2302.09664.
- Jaehoon Lee, Jascha Sohl-dickstein, Jeffrey Pennington, Roman Novak, Sam Schoenholz, and Yasaman Bahri. Deep neural networks as Gaussian processes. In *International Conference on Learning Representations*, 2018.
- Jaehoon Lee, Lechao Xiao, Samuel Schoenholz, Yasaman Bahri, Roman Novak, Jascha Sohl-Dickstein, and Jeffrey Pennington. Wide neural networks of any depth evolve as linear models under gradient descent. In *Advances in Neural Information Processing Systems*, volume 32. Curran Associates, Inc., 2019.
- Haoxi Li, Xueyang Tang, Jie Zhang, Song Guo, Sikai Bai, Peiran Dong, and Yue Yu. Causally motivated sycophancy mitigation for large language models. In *The Thirteenth International Conference on Learning Representations*.
- Qing Li, Jiahui Geng, Zongxiong Chen, Derui Zhu, Yuxia Wang, Congbo Ma, Chenyang Lyu, and Fakhri Karray. Hd-ndes: Neural differential equations for hallucination detection in llms. *arXiv preprint arXiv:2506.00088*, 2025a.
- Shaobo Li, Xiaoguang Li, Lifeng Shang, Zhenhua Dong, Chengjie Sun, Bingquan Liu, Zhenzhou Ji, Xin Jiang, and Qun Liu. How pre-trained language models capture factual knowledge? a causal-inspired analysis. *arXiv preprint arXiv:2203.16747*, 2022.
- Yucen Lily Li, Daohan Lu, Polina Kirichenko, Shikai Qiu, Tim GJ Rudner, C Bayan Bruss, and Andrew Gordon Wilson. Out-of-distribution detection methods answer the wrong questions. *arXiv* preprint arXiv:2507.01831, 2025b.

- Aixin Liu, Bei Feng, Bing Xue, Bingxuan Wang, Bochao Wu, Chengda Lu, Chenggang Zhao, Chengqi Deng, Chenyu Zhang, Chong Ruan, et al. Deepseek-v3 technical report. *arXiv preprint* arXiv:2412.19437, 2024.
- Andrey Malinin and Mark Gales. Uncertainty estimation in autoregressive structured prediction, 2021. URL https://arxiv.org/abs/2002.07650.
- Neil Mallinar, James Simon, Amirhesam Abedsoltan, Parthe Pandit, Misha Belkin, and Preetum Nakkiran. Benign, tempered, or catastrophic: Toward a refined taxonomy of overfitting. In *Advances in Neural Information Processing Systems*, volume 35, pp. 1182–1195. Curran Associates, Inc., 2022.
- Potsawee Manakul, Adian Liusie, and Mark JF Gales. Selfcheckgpt: Zero-resource black-box hallucination detection for generative large language models. *arXiv* preprint arXiv:2303.08896, 2023.
- Alexander G de G Matthews, Mark Rowland, Jiri Hron, Richard E Turner, and Zoubin Ghahramani. Gaussian process behaviour in wide deep neural networks. In *International Conference on Learning Representations*, 2018.
- Nick McKenna, Tianyi Li, Liang Cheng, Mohammad Javad Hosseini, Mark Johnson, and Mark Steedman. Sources of hallucination by large language models on inference tasks. *arXiv preprint arXiv:2305.14552*, 2023.
- William McLean. *Strongly Elliptic Systems and Boundary Integral Equations*. Cambridge University Press, 2000.
- Marko Medvedev, Gal Vardi, and Nathan Srebro. Overfitting behaviour of gaussian kernel ridgeless regression: Varying bandwidth or dimensionality. In *Advances in Neural Information Processing Systems*, volume 37, pp. 52624–52669. Curran Associates, Inc., 2024.
- Radford M Neal. Priors for infinite networks. In *Bayesian Learning for Neural Networks*, pp. 29–53. Springer, 1996.
- Charles O'Neill, Slava Chalnev, Chi Chi Zhao, Max Kirkby, and Mudith Jayasekara. A single direction of truth: An observer model's linear residual probe exposes and steers contextual hallucinations. *arXiv* preprint arXiv:2507.23221, 2025.
- OpenAI. Gpt-5 system card. Technical report, OpenAI, 2025. URL https://cdn.openai.com/gpt-5-system-card.pdf.
- Zhixuan Pan, Shaowen Wang, and Jian Li. Understanding llm behaviors via compression: Data generation, knowledge acquisition and scaling laws. *ArXiv*, abs/2504.09597, 2025. URL https://api.semanticscholar.org/CorpusID:277780691.
- Guilherme Penedo, Hynek Kydlíček, Loubna Ben allal, Anton Lozhkov, Margaret Mitchell, Colin Raffel, Leandro Von Werra, and Thomas Wolf. The fineweb datasets: Decanting the web for the finest text data at scale. In A. Globerson, L. Mackey, D. Belgrave, A. Fan, U. Paquet, J. Tomczak, and C. Zhang (eds.), Advances in Neural Information Processing Systems, volume 37, pp. 30811–30849. Curran Associates, Inc., 2024. URL https://proceedings.neurips.cc/paper\_files/paper/2024/file/370df50ccfdf8bde18f8f9c2d9151bda-Paper-Datasets\_and\_Benchmarks\_Track.pdf.

- J. Peters, Peter Buhlmann, and Nicolai Meinshausen. Causal inference by using invariant prediction: identification and confidence intervals. *Journal of the Royal Statistical Society: Series B (Statistical Methodology)*, 78, 2015. URL https://api.semanticscholar.org/CorpusID:36882285.
- Qwen, :, An Yang, Baosong Yang, Beichen Zhang, Binyuan Hui, Bo Zheng, Bowen Yu, Chengyuan Li, Dayiheng Liu, Fei Huang, Haoran Wei, Huan Lin, Jian Yang, Jianhong Tu, Jianwei Zhang, Jianxin Yang, Jiaxi Yang, Jingren Zhou, Junyang Lin, Kai Dang, Keming Lu, Keqin Bao, Kexin Yang, Le Yu, Mei Li, Mingfeng Xue, Pei Zhang, Qin Zhu, Rui Men, Runji Lin, Tianhao Li, Tianyi Tang, Tingyu Xia, Xingzhang Ren, Xuancheng Ren, Yang Fan, Yang Su, Yichang Zhang, Yu Wan, Yuqiong Liu, Zeyu Cui, Zhenru Zhang, and Zihan Qiu. Qwen2.5 technical report, 2025. URL https://arxiv.org/abs/2412.15115.
- Abhilasha Ravichander, Shrusti Ghela, David Wadden, and Yejin Choi. Halogen: Fantastic llm hallucinations and where to find them. *arXiv preprint arXiv:2501.08292*, 2025.
- Baochang Ren, Shuofei Qiao, Wenhao Yu, Huajun Chen, and Ningyu Zhang. Knowrl: Exploring knowledgeable reinforcement learning for factuality. *arXiv preprint arXiv:2506.19807*, 2025.
- Aleksandr Reznikov and Edward B Saff. The covering radius of randomly distributed points on a manifold. *International Mathematics Research Notices*, 2016(19):6065–6094, 2016.
- James Benjamin Simon, Sajant Anand, and Mike Deweese. Reverse engineering the neural tangent kernel. In *Proceedings of the 39th International Conference on Machine Learning*, volume 162 of *Proceedings of Machine Learning Research*, pp. 20215–20231. PMLR, PMLR, 2022.
- Anikait Singh, Sheryl Hsu, Kyle Hsu, Eric Mitchell, Stefano Ermon, Tatsunori Hashimoto, Archit Sharma, and Chelsea Finn. Fspo: Few-shot preference optimization of synthetic preference data in llms elicits effective personalization to real users. *arXiv* preprint arXiv:2502.19312, 2025.
- Gaurang Sriramanan, Siddhant Bharti, Vinu Sankar Sadasivan, Shoumik Saha, Priyatham Kattakinda, and Soheil Feizi. Llm-check: Investigating detection of hallucinations in large language models. *Advances in Neural Information Processing Systems*, 37:34188–34216, 2024.
- Kai Sun, Yifan Ethan Xu, Hanwen Zha, Yue Liu, and Xin Luna Dong. Head-to-tail: How knowledgeable are large language models (llms)? aka will llms replace knowledge graphs? *arXiv preprint arXiv:2308.10168*, 2023.
- Yiyou Sun, Yu Gai, Lijie Chen, Abhilasha Ravichander, Yejin Choi, and Dawn Song. Why and how llms hallucinate: Connecting the dots with subsequence associations. *arXiv* preprint arXiv:2504.12691, 2025.
- Amir Taubenfeld, Tom Sheffer, Eran Ofek, Amir Feder, Ariel Goldstein, Zorik Gekhman, and Gal Yona. Confidence improves self-consistency in llms. *arXiv preprint arXiv:2502.06233*, 2025.
- SMTI Tonmoy, SM Zaman, Vinija Jain, Anku Rani, Vipula Rawte, Aman Chadha, and Amitava Das. A comprehensive survey of hallucination mitigation techniques in large language models. *arXiv preprint arXiv:2401.01313*, 6, 2024.
- Antonio Torralba and Alexei A. Efros. Unbiased look at dataset bias. *CVPR 2011*, pp. 1521–1528, 2011. URL https://api.semanticscholar.org/CorpusID:2777306.

- Jindong Wang, Cuiling Lan, Chang Liu, Yidong Ouyang, Tao Qin, Wang Lu, Yiqiang Chen, Wenjun Zeng, and Philip S Yu. Generalizing to unseen domains: A survey on domain generalization. *IEEE transactions on knowledge and data engineering*, 35(8):8052–8072, 2022.
- Wenjia Wang, Xiaowei Zhang, and Lu Zou. Regret optimality of GP-UCB, 2023. URL https://arxiv.org/abs/2312.01386.
- Zhiwei Wang, Zhongxin Liu, Ying Li, Hongyu Sun, Meng Xu, and Yuqing Zhang. Kshseek: Data-driven approaches to mitigating and detecting knowledge-shortcut hallucinations in generative models. *arXiv* preprint arXiv:2503.19482, 2025.
- Jason Wei, Nguyen Karina, Hyung Won Chung, Yunxin Joy Jiao, Spencer Papay, Amelia Glaese, John Schulman, and William Fedus. Measuring short-form factuality in large language models. arXiv preprint arXiv:2411.04368, 2024.
- Jerry Wei, Da Huang, Yifeng Lu, Denny Zhou, and Quoc V Le. Simple synthetic data reduces sycophancy in large language models. *arXiv preprint arXiv:2308.03958*, 2023.
- Holger Wendland. Piecewise polynomial, positive definite and compactly supported radial functions of minimal degree. *Advances in Computational Mathematics*, 4:389–396, 1995.
- Holger Wendland. Scattered Data Approximation. Cambridge University Press, 2004.
- Zong-min Wu and Robert Schaback. Local error estimates for radial basis function interpolation of scattered data. *IMA Journal of Numerical Analysis*, 13(1):13–27, 1993.
- Tianyang Xu, Shujin Wu, Shizhe Diao, Xiaoze Liu, Xingyao Wang, Yangyi Chen, and Jing Gao. Sayself: Teaching Ilms to express confidence with self-reflective rationales, 2024. URL https://arxiv.org/abs/2405.20974.
- An Yang, Anfeng Li, Baosong Yang, Beichen Zhang, Binyuan Hui, Bo Zheng, Bowen Yu, Chang Gao, Chengen Huang, Chenxu Lv, et al. Qwen3 technical report. *arXiv preprint arXiv:2505.09388*, 2025.
- Greg Yang. Tensor programs II: Neural tangent kernel for any architecture, 2020. URL https://arxiv.org/abs/2006.14548.
- Greg Yang and Etai Littwin. Tensor programs IIb: Architectural universality of neural tangent kernel training dynamics. In *International Conference on Machine Learning*, pp. 11762–11772. PMLR, 2021.
- Wenqian Ye, Guangtao Zheng, Xu Cao, Yunsheng Ma, and Aidong Zhang. Spurious correlations in machine learning: A survey. *arXiv preprint arXiv:2402.12715*, 2024.
- Zhangyue Yin, Qiushi Sun, Qipeng Guo, Jiawen Wu, Xipeng Qiu, and Xuanjing Huang. Do large language models know what they don't know? *arXiv preprint arXiv:2305.18153*, 2023.
- Yu Yuan, Lili Zhao, Kai Zhang, Guangting Zheng, and Qi Liu. Do llms overcome shortcut learning? an evaluation of shortcut challenges in large language models. *arXiv preprint arXiv:2410.13343*, 2024.
- Hanning Zhang, Shizhe Diao, Yong Lin, Yi Fung, Qing Lian, Xingyao Wang, Yangyi Chen, Heng Ji, and Tong Zhang. R-tuning: Instructing large language models to say 'i don't know'. In *Proceedings of the 2024 Conference of the North American Chapter of the Association for Computational Linguistics: Human Language Technologies (Volume 1: Long Papers)*, pp. 7106–7132, 2024.

- Haobo Zhang, Weihao Lu, and Qian Lin. The phase diagram of kernel interpolation in large dimensions. *Biometrika*, 112(1):asae057, 11 2025a.
- Muru Zhang, Ofir Press, William Merrill, Alisa Liu, and Noah A Smith. How language model hallucinations can snowball. *arXiv preprint arXiv:2305.13534*, 2023.
- Yue Zhang, Yafu Li, Leyang Cui, Deng Cai, Lemao Liu, Tingchen Fu, Xinting Huang, Enbo Zhao, Yu Zhang, Yulong Chen, et al. Siren's song in the ai ocean: A survey on hallucination in large language models. *Computational Linguistics*, pp. 1–46, 2025b.
- Kaiyang Zhou, Ziwei Liu, Yu Qiao, Tao Xiang, and Chen Change Loy. Domain generalization: A survey. *IEEE transactions on pattern analysis and machine intelligence*, 45(4):4396–4415, 2022.
- Yuhang Zhou, Paiheng Xu, Xiaoyu Liu, Bang An, Wei Ai, and Furong Huang. Explore spurious correlations at the concept level in language models for text classification. *arXiv* preprint arXiv:2311.08648, 2023.
- Andy Zou, Long Phan, Sarah Chen, James Campbell, Phillip Guo, Richard Ren, Alexander Pan, Xuwang Yin, Mantas Mazeika, Ann-Kathrin Dombrowski, et al. Representation engineering: A top-down approach to ai transparency. *arXiv preprint arXiv:2310.01405*, 2023.

## **A** Additional Related Works

Table 1: Hallucination Detection Methods

Method Cate- gory	Method	Description and Details	
Logits-based	Perplexity(Malinin & Gales, 2021; Kuhn et al., 2023)	Measures how well the model predicts the next token. A higher perplexity usually indicates lower model confidence. $\mathrm{PPL} = \exp\left(-\frac{1}{N}\sum_{i=1}^N \log p(x_i\mid x_{< i})\right)$	
	Logit Entropy(Malinin & Gales, 2021)	Quantifies uncertainty by measuring the entropy over the predicted token distribution. Larger values indicate higher uncertainty. $H(\mathbf{z}) = -\sum_{j=1}^{ V } \sigma(\mathbf{z})_j \log \sigma(\mathbf{z})_j$	
	Window Entropy (Sriramanan et al., 2024)	where $\sigma(\cdot)$ is the softmax over logits $\mathbf{z}$ . Computes the logit entropy within a sliding window to capture local uncertainty patterns. For each position $i$ : $H_i = -\sum_{v \in V} p(v \mid x_{< i}) \log p(v \mid x_{< i})$	
Hidden-state- based	Attention Score(Sriramanan et al., 2024)	Uses the log-determinant of kernel similarity maps from self-attention heads as a feature. A higher score suggests a higher probability of hallucination. $\log \det(Ker_i) = \sum_{j=1}^m \log Ker_i^{jj}$	
		(Continued on next page)	

Method Cate- gory	Method	Description and Details		
	Linear Probing of Hidden States(O'Neill et al., 2025)	Trains a lightweight classifier (e.g., logistic regression) on hidden representations to identify hallucinations.  Common feature types include:  • Average input hidden state  • Last-token input hidden state  • Average output hidden state  • Last-token output hidden state		
Confidence- based	Self- Consistency(Kuhn et al., 2023)	Measures self-consistency by generating multiple responses for the same prompt and assessing their agreement. Identify the most frequent answer among all generations and compute the proportion of outputs matching it. A higher proportion indicates stronger self-consistency and a lower likelihood of hallucination.		
	Self-Confidence(Xu et al., 2024)	Obtains the model's explicit confidence score by modifying the prompt to request a self-assessment of its answer. The model is asked to provide both the response and a confidence value indicating how certain it is about its answer.		

#### **A.1** Detailed Taxonomy and Benchmarks for Hallucination

Here, we expand on the classification and evaluation of hallucinations, supplementing the discussion in Section 2.1.

**A Detailed Taxonomy of Hallucinations** A common taxonomy arranges hallucinations along several largely independent axes to provide a shared vocabulary for analysis:

- Factuality vs. Faithfulness: This axis distinguishes errors measured against external, established world knowledge (Factuality) from those that contradict information supplied in the prompt or source context (Faithfulness) (Ji et al., 2023; Zhang et al., 2025b).
- **Intrinsic vs. Extrinsic:** This separates errors attributable to a model's flawed parametric knowledge (Intrinsic) from those arising due to failures in retrieving or grounding on external information (Extrinsic) (Ji et al., 2023; Tonmoy et al., 2024).
- **Granularity:** This axis defines the unit of analysis, which can range from a specific claim or span, up to the level of a full passage or task output. This helps clarify the intended target of a method (e.g., detection, abstention, or correction) (Tonmoy et al., 2024).

Alternative categorizations, such as input-conflicting, context-conflicting, or fact-conflicting, are also used in recent surveys and are broadly consistent with these primary axes (Zhang et al., 2025b).

Causes of Hallucinations: Evidence and Analyses Hallucinations arise from a complex interplay of factors, but are frequently traced to statistical artifacts in the training corpus. Spurious correlations and surface co-occurrences can create powerful, shortcut-like associations that overshadow genuine dependencies (Li et al., 2022; Sun et al., 2023). These issues are often exacerbated by learning objectives that discourage uncertainty and decoding dynamics that amplify early errors (Yin et al., 2023; Zhang et al., 2023).

Two recent lines of work provide theoretical explanations for why hallucinations are so persistent. A mechanistic view hypothesizes that hallucination occurs when the cumulative association for a fallacious output subsequence, often driven by a dominant trigger, outweighs that of a faithful one (Sun et al., 2025). Complementing this, recent theoretical studies reveal fundamental trade-offs between maintaining expressive generation and avoiding hallucinations, suggesting that unavoidable error exist even for perfectly calibrated models and clean data (Kalai et al., 2025; Kalai & Vempala, 2024; Kalavasis et al., 2025).

Taken together, these analyses suggest that shortcut-like statistical regularities may systematically overpower faithful associations, producing high-consistency, high-confidence errors that persist with scale and resist defenses predicated on uncertainty. Motivated by these observations, we examine spurious correlations as a primary driver and evaluate whether confidence-, consistency-, and probe-based detectors remain reliable as shortcut strength is varied, following measurement principles that emphasize causal tracing across contexts and atomic-fact evaluation (Sun et al., 2025; Kalai et al., 2025).

**Benchmarks for Atomic Factuality** To improve comparability and verifiability across tasks, recent benchmarks have been developed to decompose model outputs into atomic factual units and apply programmatic checks.

- **SimpleQA** evaluates whether models "know what they know" by rewarding both correct answers and appropriate abstention on unanswerable questions. This design allows for the separate measurement of a model's precision, coverage, and calibration (Wei et al., 2024).
- HALoGEN verifies atomic facts asserted in a model's output against a set of trusted sources. It also
  introduces a fine-grained, three-category error schema (misrecall, incorrect parametric knowledge,
  and fabrication) to support more consistent and insightful cross-domain analysis of hallucinatory behavior (Ravichander et al., 2025).

#### A.2 A Catalog of Hallucination Detection and Mitigation Methods

This section provides brief descriptions of the specific methods for hallucination detection and mitigation that we cite in Section 2.2.

**Selective Answering and Abstention** These methods encourage models to respond only when confident.

- **ConfQA** operationalizes this idea at the atomic-fact level via instruction framing and fine-tuning, improving the mapping between verbalized confidence and factual accuracy on short-form questions (Huang et al., 2025).
- **R-Tuning** explicitly instructs models to say "I don't know" when uncertain to strengthen abstention capabilities (Zhang et al., 2024).
- **Self-alignment** trains models to explain why a question is unanswerable, providing a more reasoned form of refusal (Deng et al., 2024).

**Confidence-Weighted Reasoning and Self-Consistency** These methods aggregate multiple outputs, prioritizing those with higher confidence.

- Confidence Improves Self-Consistency (CISC) performs a confidence-weighted vote over sampled solutions to reduce the sample complexity of self-consistency (Taubenfeld et al., 2025).
- **Deep Think with Confidence (DeepConf)** maintains a lightweight, local confidence signal during generation to prune low-quality trajectories and enable early stopping, improving the accuracy-efficiency trade-off (Fu et al., 2025).

**Post hoc and Internal Detectors** These methods aim to identify hallucinations in generated text or internal model states.

- **SelfCheckGPT** (External) samples alternative continuations from the language model and flags inconsistency as a proxy for unreliability (Manakul et al., 2023).
- **TTPD** (External) frames falsehood detection as a text-classification problem, identifying a low-dimensional "truth subspace" that can generalize across prompts and tasks (Bürger et al., 2024).
- **HD-NDEs** (Internal) model the latent trajectory dynamics during generation with neural differential equations, mapping them to a classifier to flag non-factual statements (Li et al., 2025a).
- Linear Probing / Observer Models (Internal) use simple linear probes on residual-stream activations to separate faithful from hallucinated spans in a single forward pass, identifying transferable directions that can influence hallucination rates (O'Neill et al., 2025).

**Training-Time Objectives** These methods modify the learning process to improve factuality.

- **Beyond Binary Rewards (RLCR)** augments correctness with a proper scoring term (e.g., Brier score) to achieve calibrated confidence with theoretical guarantees (Damani et al., 2025).
- **Knowledge-enhanced RL (KnowRL)** integrates a factuality reward based on knowledge verification into slow-thinking training loops to encourage fact-based reasoning (Ren et al., 2025).

#### A.3 Additional Factors in Shortcut Learning and Robustness

This section provides further context on the literature concerning the causes of hallucinations and robustness, supplementing Sections 2.3 and 2.4.

**Further Contributing Factors to Hallucination** Beyond spurious correlations, the literature points to several other contributing factors. On the corpus side, these include long-tailed coverage, which leaves rare facts weakly supported (Sun et al., 2023), and data asymmetries like the reversal curse (Berglund et al., 2023). On the objective side, models often fail to recognize what they do not know (Yin et al., 2023) and can be encouraged by alignment to agree with users rather than convey uncertainty (Wei et al., 2023). Finally, exposure bias in sequence learning can compound local errors as generation unfolds, a phenomenon sometimes called error snowballing (Bengio et al., 2015; Zhang et al., 2023).

**Method Families in Domain Generalization** The field of domain generalization (DG) aims to learn models that are robust to distribution shifts, such as those caused by shortcut features. Surveys in this area typically organize methods into three high-level families: (i) data manipulation (e.g., augmentation), (ii) representation learning and regularization for achieving invariance, and (iii) optimization techniques like meta-learning (Zhou et al., 2022; Wang et al., 2022). Countermeasures against spurious correlations, such as group-robust training and invariant-learning principles, emerge from this literature and aim to suppress reliance on non-causal features during training (Ye et al., 2024; Zhou et al., 2022).

Shortcut Learning and Robustness Shortcut learning refers to models exploiting superficial but predictive correlations instead of the intended causal signals, leading to good performance on i.i.d. benchmarks but failures under distribution shift (Geirhos et al., 2020a). This challenge is a central focus of domain generalization, which studies how to build models that are robust to such spurious correlations (Zhou et al., 2022; Ye et al., 2024). Critically, this framing reveals why simply detecting distribution shifts is insufficient: many OOD detectors fail when a model encounters a strong shortcut feature, because the model remains highly confident in its (wrong) prediction (Li et al., 2025b).

We argue that high-confidence hallucinations in LLMs are a manifestation of this exact problem. In our setting, shortcut-like statistical associations in training corpora act as spurious features, inducing high-consistency, high-confidence errors that evade standard detectors and persist with scale (Geirhos et al., 2020a). Our experiments, therefore, instantiate this robustness lens for LLMs. We systematically control the strength of spurious correlations and test whether common hallucination detectors—based on confidence, consistency, and internal probes—remain reliable under these challenging conditions, using atomic-fact measurements tailored to language generation.

#### **B** Proofs

To obtain our main results, we impose the definition of RKHS and the following assumptions.

**Definition 1.** The kernel function k(x, x') is positive definite for any  $x, x' \in \mathcal{X}$ . The objective function  $f \in \mathcal{H}_k$  lives in the reproducing kernel Hilbert space (RKHS) induced by k. The RKHS endowed with the inner product  $\langle \cdot, \cdot \rangle_{\mathcal{H}_k}$  is defined as

$$\mathcal{H}_k \coloneqq \left\{ f = \sum_{i=1}^{\infty} c_i k(\cdot, x_i) : (c_1, c_2, \dots) \subset \mathbb{R}, \quad (x_1, x_2, \dots) \subset \mathcal{X}, \quad \text{ such that } \right\}$$

$$||f||_{\mathcal{H}_k}^2 := \lim_{n \to \infty} \left\| \sum_{i=1}^n c_i k(\cdot, x_i) \right\|_{\mathcal{H}_k}^2 = \sum_{i,j=1}^\infty c_i c_j k(x_i, x_j) < \infty \right\},$$

and for any  $f,g\in\mathcal{H}_k$  with  $f=\sum_{i=1}^\infty c_i k(\cdot,x_i)$  and  $g=\sum_{j=1}^\infty c_j' k(\cdot,x_j')$ ,

$$\langle f, g \rangle_{\mathcal{H}_k} \coloneqq \sum_{i,j=1}^{\infty} c_i c'_j k(x_i, x'_j).$$

**Assumption 1.** The kernel k is translation-invariant, i.e.,  $k(x,x') = \Psi(x-x')$  for some  $\nu$ -Holder continuous function  $\Psi: \mathbb{R}^{d+1} \to \mathbb{R}$  such that  $|\Psi(x) - \Psi(x')| \le A ||x-x'||_2^{\nu}$  for some constants  $A, \nu > 0$ .

**Assumption 2.** The RKHS  $\mathcal{H}_k(\mathbb{S}^d)$  generated by the kernel k is norm equivalent to the Sobolev space  $W_2^s(\mathbb{S}^d)$  of finite smoothness s > (d+1)/2.

**Assumption 3.** The target function  $f^*$  lies in the RKHS  $\mathcal{H}_k(\mathbb{R}^d)$ , with  $||f^*||_{\mathcal{H}_k} \leq B$  for some constant B > 0.

**Assumption 4.** For the case of interpolation, the kernel matrix  $k(X_N, X_N)$  is invertible.

Note that dot-product kernels on  $\mathbb{S}^d$  are all radius basis function kernels, hence translation-invariant. So that the above assumptions are also satisfied by neural kernels such as NNGP and NTK. Assumption 3 avoids the Gibbs phenomenon at the boundary between the correlation and noisy regions, ensuring that the target function can be well approximated by functions in the RKHS. Assumption 4 guarantees the uniqueness of the kernel interpolation solution.

#### **B.1** Kernel Ridge Regression with Fixed Bandwidth

**Theorem 2.** Under Assumptions 1-3, there exist some constants  $C_0, C_1, C_2, C_3, N_0 > 0$  such that, for any  $\delta \in (0, 1)$  and  $N \ge N_0$ , define the uniform upper confidence bound as

$$U_N^{\delta} := C_0 C_2^{1/2} \left( \frac{\ln(N/2)}{C_3 N} \right)^{\frac{2s - d - 1}{2d}} \sqrt{\ln(1 + \lambda N) \ln(e + 2C_1/\delta)}.$$

Then, the following holds with probability at least  $1 - \delta$ ,

$$\inf_{x \in \mathcal{C}} |f_N(x)| \ge 0.98 - U_N^{\delta}, \quad \sup_{x \in \mathcal{N}} |f_N(x)| \le U_N^{\delta}.$$

Therefore, for any threshold  $\rho \in (0, 0.98)$ , if N is sufficiently large, then

$$\mathbb{P}\left(\left\{|f_N(x)| \ge \rho, \ \forall x \in \mathcal{C}\right\} \cap \left\{|f_N(x')| < \rho, \ \forall x' \in \mathcal{N}\right\}\right) \ge 1 - \delta,$$

which indicates that any hallucination detection criterion with a fixed  $\rho$  fails in both the correlation and noisy regions.

Theorem 2 shows that as the training set size increases, in the correlation region, the model output tends to be closer in absolute value to the sample labels, while in the noisy region, the output deviates from the sample labels. Therefore, KRR cannot detect hallucinations in any region. This is because the regularization term enforces smoothness on the predictor, causing it to converge to the target function as N goes to infinity, while ignoring all "noisy" information, even though such noise may be considered memorized facts in practice.

**Lemma 3.** Under Assumptions 1-3, for any  $N \ge 1$ ,  $\delta \in (0,1)$ ,  $\{x_1,\ldots,x_N\} \subset \mathbb{S}^d$ , and independent sub-Gaussian random variables  $\{\varepsilon_1,\ldots,\varepsilon_N\}$  with mean zero and variance proxy  $\varsigma^2$ , there exist constants  $C_0,C_1>0$  only depending on k, d and  $\varsigma$  such that

$$\mathbb{P}\left(|f_N(x) - f^*(x)| \le C_0 \sigma_N(x) \sqrt{\ln(1 + \lambda N) \ln(e + C_1/\delta)}, \quad \text{for all } x \in \mathbb{S}^d\right) \ge 1 - \delta.$$

*Proof.* The original statement in Wang et al. (2023) holds when the domain is assumed to be compact and convex. The convexity assumption can be removed as follows: First, a classical approach is to extend the domain to a compact set with Lipschitz boundary and satisfying the interior cone condition (Wendland, 2004). Second, by the Sobolev Extension Theorem (McLean, 2000), any function in  $W_2^s(\mathbb{S}^d)$  can be extended to a function in  $W_2^{s+1/2}(B_{d+1})$ , where  $B_{d+1}$  is the unit ball containing  $\mathbb{S}^d$ . The extension operator is linear and bounded, so the norm equivalence in Assumption 2 still holds up to a constant. Therefore, the proof of Theorem 1 in Wang et al. (2023) remains valid.

**Definition 2.** The *fill distance*, also known as covering radius or mesh norm, is commonly used to measure how well a sample sequence covers the entire space. The fill distance is then calculated as:

$$h_{\mathcal{X},X_N} \coloneqq \sup_{x \in \mathcal{X}} \inf_{x_i \in X_N} \|x - x_i\|.$$

For simplicity, we denote  $h_N = h_{\mathcal{X}, X_N}$  in the following.

**Lemma 4** (Theorem 5 in Wu & Schaback (1993)). Under Assumption 2, there exist constants  $C_2, h_0 > 0$  such that, for an arbitrary dataset  $X_N = \{x_1, \dots, x_N\}$  satisfying  $h_N \le h_0$ ,

$$\sigma_N^2(x) \le C_2 h_N^{2s-d-1}.$$

Let  $\mathscr{H}_d$  be the d-dimensional Hausdorff measure,  $\mu(\cdot) = \mathbb{1}_{\mathbb{S}^d}(\cdot)\mathscr{H}_d(\cdot)/\mathscr{H}_d(\mathbb{S}^d)$  be the uniform probability measure on  $\mathbb{S}^d$ . Adapted from Theorem 2.1 and Corollary 3.4 in Reznikov & Saff (2016), we have a non-asymptotic tail bound on the fill distance for i.i.d. sampled data points on the sphere.

**Lemma 5.** Suppose  $X_N = \{x_1, \dots, x_N\}$  are independently uniformly sampled from  $\mathbb{S}^d$ . There exist a constant  $C_3$  only depends on d such that, for any  $\delta \in (0,1)$  and  $N \geq 3$ , with probability at least  $1 - \delta$ ,

$$h_N \le \left(\frac{\ln(N\delta)}{C_3N}\right)^{1/d}.$$

*Proof.* For any fixed  $x \in \mathbb{S}^d$ , the Ahlfors-David regularity (David & Semmes, 1993) of the sphere implies that there exists a constant  $\omega_d > 0$  such that

$$\mathscr{H}_d(B(x,r)\cap\mathbb{S}^d)\geq \omega_d r^d,\quad \forall r\in\left(0,\operatorname{diam}(\mathbb{S}^d)\right],$$

Suppose  $t < \operatorname{diam}(\mathbb{S}^d) = 2$ , if  $h_N > t$ , then there exists  $z \in \mathbb{S}^d$  such that  $B(z,t) \cap X_N = \emptyset$ . Let  $\mathscr{E}_{t/2}$  be any maximal t/2-separated subset of  $\mathbb{S}^d$ , i.e., for any  $x, x' \in \mathscr{E}_{t/2}$ ,  $\|x - x'\| \ge t/2$ . So there exists  $x \in B(z, t/2) \cap \mathscr{E}_{t/2}$ , then  $B(x, t/4) \cap X_N = \emptyset$ . Therefore,

$$\mathbb{P}(h_N > t) \leq \mathbb{P}\left(\exists x \in \mathscr{E}_{t/2}, B(x, t/4) \cap X_N = \varnothing\right)$$

$$= \mathbb{P}\left(\bigcup_{x \in \mathscr{E}_{t/2}} \bigcap_{x_i \in X_N} \left\{x_i \notin B(x, t/4)\right\}\right)$$

$$\leq \operatorname{card}(\mathscr{E}_{t/2}) \left(1 - \frac{\omega_d(t/4)^d}{\mathscr{H}_d(\mathbb{S}^d)}\right)^N,$$

where  $\operatorname{card}(\mathcal{E}_{\cdot})$  is the packing number satisfying

$$\mathscr{H}_d(\mathbb{S}^d) \ge \sum_{x \in \mathscr{E}_{t/2}} \mathscr{H}_d(B(x, t/4) \cap \mathbb{S}^d) \ge \operatorname{card}(\mathscr{E}_{t/2})\omega_d(t/4)^d.$$

So that

$$\mathbb{P}(h_N > t) \leq \frac{\mathcal{H}_d(\mathbb{S}^d)}{\omega_d(t/4)^d} \left( 1 - \frac{\omega_d(t/4)^d}{\mathcal{H}_d(\mathbb{S}^d)} \right)^N$$

$$\leq \frac{\mathcal{H}_d(\mathbb{S}^d)}{\omega_d(t/4)^d} \exp\left( -\frac{\omega_d(t/4)^d}{\mathcal{H}_d(\mathbb{S}^d)} N \right)$$

$$= (Ct^d)^{-1} \exp(-Ct^d N).$$

Where  $C := \omega_d/(4^d \mathcal{H}_d(\mathbb{S}^d))$  is a positive constant only depending on d.

Let  $\delta = (Ct^d)^{-1} \exp(-Ct^dN)$ , then  $t = (W(N/\delta)/CN)^{1/d}$ , where  $W(\cdot)$  is the Lambert W function. Note that  $W(x) < \ln(x)$  when x > e, so if  $N > \delta e$ , then with probability at least  $1 - \delta$ ,

$$h_N \le \left(\frac{\ln(N\delta)}{CN}\right)^{1/d},$$

which completes the proof.

*Proof of Theorem* 2. By Lemma 5, for any  $\delta \in (0,1)$  and  $N \geq 3$ , the following holds with probability at least  $1 - \delta/2$ ,

$$h_N^d \le \frac{\ln(N\delta/2)}{C_3 N} \le \frac{\ln(N/2)}{C_3 N}.$$

To satisfy the condition  $h_N \leq h_0$  in Lemma 4, by the monotonicity of  $\ln(x)/x$ , it suffices to take  $N \geq N_0 := \max\{2\ln(1/(2C_3h_0^d))/C_3h_0^d, 3\}$ . Conditioned on the above  $X_N$ , by Lemma 3 and Lemma 4, with probability at least  $1 - \delta/2$ , the following holds for all  $x \in \mathbb{S}^d$ ,

$$|f_N(x) - f^*(x)| \le C_0 \sigma_N(x) \sqrt{\ln(1 + \lambda N) \ln(e + 2C_1/\delta)}$$

$$\le C_0 C_2^{1/2} \left(\frac{\ln(N/2)}{C_3 N}\right)^{\frac{2s - d - 1}{2d}} \sqrt{\ln(1 + \lambda N) \ln(e + 2C_1/\delta)} := U_N^{\delta}.$$

By the union bound, with probability at least  $1 - \delta$ , the above holds for all  $x \in \mathbb{S}^d$ . Combining with the definition of  $f^*$ , we have

$$\inf_{x \in \mathcal{C}} |f_N(x)| \ge 0.98 - U_N^{\delta}, \quad \sup_{x \in \mathcal{N}} |f_N(x)| \le U_N^{\delta}.$$

#### **B.2** Kernel Ridge Regression with Decaying Bandwidth

**Definition 3.** The *separation distance*, is a measure links to packing in the space. The separation distance is then calculated as:

$$q_{\mathcal{X},X_N} \coloneqq \inf_{x_i \neq x_j \in X_N} \|x_i - x_j\|.$$

For simplicity, we denote  $q_N = q_{\mathcal{X},X_N}$  in the following. Note that when  $X_N$  are sampled i.i.d. uniformly, the separation distance is of the same order as the fill distance and thus, up to a constant factor, has the same tail bound.

**Lemma 6** (Theorem 2.2 in Reznikov & Saff (2016)). Under the same conditions as Lemma 5, there exist constants  $C_1$ ,  $C_2$  only depends on d such that,

$$\lim_{N\to\infty} \mathbb{P}\left(h_N \ge C_1 \left(\frac{\ln N - C_2 \ln \ln N}{N}\right)^{1/d}\right) = 1.$$

If we set the bandwidth of KRR sufficiently small, the model is forced to memorize all data points. However, such a predictor is inconsistent (i.e., excess risk is bounded away from zero). The following Theorem 7 gives an intuitive explanation for this phenomenon.

**Theorem 7.** Suppose Assumptions 1-3 hold. Further, assume the kernel function has compact support, define as  $k_{\ell_N}(x,x') := \Psi((x-x')/\ell_N)$ , where  $\Psi$  is supported on B(0,1) (e.g., Wendland kernel (Wendland, 1995)) and  $\ell_N > 0$  is the bandwidth. Let  $\ell_N = o(N^{1/d})$ , there exists a constant  $\rho \in (0,1)$  depending on  $\lambda$  such that  $\lim_{\lambda \to 0} \rho = 1$  and

$$\lim_{N \to \infty} \mathbb{P}(|f_N(x_i)| \ge \rho) = 1, \quad \forall i = 1, \dots, N.$$

However,

$$\lim_{N \to \infty} \mathbb{P}\left(f_N(x) \neq 0\right) = 0,$$

which indicates that even within the correlation region, the predictor fails to learn any correlation.

*Proof.* By Lemma 6, for sufficiently large N, we have  $\ell_N < q_N$  holds with probability 1. Therefore, the kernel matrix  $k_{\ell_N}(X_N,X_N)$  is diagonal dominant with diagonal entries being  $\Psi(0)$  and off-diagonal entries being zero. So that

$$f_N(x_i) = k_{\ell_N}(x_i, X_N)(k_{\ell_N}(X_N, X_N) + N\lambda I_N)^{-1} Y_N = \frac{\Psi(0)}{\Psi(0) + N\lambda} y_i.$$

Let  $\rho = |\Psi(0)|/(|\Psi(0)| + \lambda)$ , then  $|f_N(x_i)| \ge \rho$  for all  $i = 1, \dots, N$ .

On the other hand, the result is direct by the compact support of the kernel and the Ahlfors-David regularity,

$$\mathbb{P}(f_N(x) \neq 0) \leq N\mu(B(x, \ell_N)) \to 0$$
, as  $N \to \infty$ .

Theorem 7 shows that, in order to memorize all data points, the predictor forgoes learning correlations, leading to poor performance even within the correlation region. Setting  $\lambda = 0$  reduces KRR to kernel interpolation, whose test error behavior in fixed dimensions is known as *tempered overfitting* for kernels with polynomially decaying spectra (e.g., Laplacian kernels), and *catastrophic overfitting* for kernels with exponentially decaying spectra (e.g., Gaussian kernels) (Mallinar et al., 2022; Cheng et al., 2024b).

#### **B.3** Kernel Ridgeless Regression with Benign Overfitting

**Theorem 8.** Suppose Assumptions 1-4 hold. Further, assume either

- $C_1 d^{\gamma} \leq N \leq C_2 d^{\gamma}$  for some  $\gamma \in \mathbb{R}_+ \setminus \mathbb{Z}$  and  $C_1, C_2 > 0$ ; or
- the kernel function is define as  $k_{c_N,\gamma_N}(x,x') := \tilde{k}(x,x') + c_N \check{k}_{\gamma_N}(x,x')$ , where  $\tilde{k}$  is a universal kernel,  $\check{k}_{\gamma_N}$  is the Laplace kernel with bandwidth  $\gamma_N > 0$ ,  $c_N \to 0$ ,  $Nc_N^4 \to \infty$ , and  $\gamma_N \le N^{-3/d}(7 \ln N)^{-1}$ .

Then for any  $\delta \in (0,1)$ , there exist constants  $C_0, N_0, \alpha > 0$  such that for any  $N \geq N_0$ , if we define the uniform upper confidence bound as  $U_N^{\delta} \coloneqq C_0 N^{-\alpha}$ , the following holds

$$\mathbb{P}\left(\mathbb{E}_{D_N}\left[|f_N(x)| \ge 0.98 - U_N^{\delta}\right]\right) \ge 1 - \delta, \quad \text{for all } x \in \mathcal{C},$$

$$\mathbb{P}\left(\mathbb{E}_{D_N}\left[|f_N(x)| \le U_N^{\delta}\right]\right) \ge 1 - \delta, \quad \text{for all } x \in \mathcal{N}.$$

Therefore, for any threshold  $\rho \in (0, 0.98)$ ,

$$\lim_{N \to \infty} \inf \mathbb{P}\left(\mathbb{E}_{D_N}\left[|f_N(x)| \ge \rho\right]\right) \ge 1 - \delta, \quad \text{for all } x \in \mathcal{C},$$

which indicates that any hallucination detection criterion with a fixed  $\rho$  fails in the correlation regions.

To prove Theorem 8, we first define the excess risk of the kernel interpolation estimator  $f_N$  by

$$\mathcal{E}_N := \mathbb{E}_{x,D_N} \left[ (f_N(x) - f^*(x))^2 \right].$$

A classical approach to achieving benign overfitting with kernel interpolation is to increase the input dimensionality (Barzilai & Shamir, 2024; Zhang et al., 2025a; Medvedev et al., 2024), as detailed in Proposition 9.

**Proposition 9** (Corollary 3.0.3 in Zhang et al. (2025a)). Let  $C_1 d^{\gamma} \leq N \leq C_2 d^{\gamma}$  for some  $\gamma \in \mathbb{R}_+ \setminus \mathbb{Z}$  and  $C_1, C_2 > 0$ . Under some technical assumptions on the spectrum of kernel k and the smoothness of  $f^*$ , there exists a constant  $\alpha > 0$  only depending on  $\gamma, k$  and d, such that the excess risk  $\mathcal{E}_N$  of kernel interpolation estimator  $f_N$  satisfies

$$\mathcal{E}_N = O_{\mathbb{P}}(N^{-\alpha})$$
 as  $N, d \to \infty$ .

While in finite dimensions, the benign overfitting of kernel interpolation can be achieved by just adding a sharp kernel spike to a common kernel (Haas et al., 2023).

**Proposition 10** (Theorem G.5 in Haas et al. (2023)). Under Assumptions 1-3. Further, assume the kernel function is define as  $k_{c_N,\gamma_N}(x,x') := \tilde{k}(x,x') + c_N \check{k}_{\gamma_N}(x,x')$ , where  $\tilde{k}$  is a universal kernel,  $\check{k}_{\gamma_N}$  is the Laplace kernel with bandwidth  $\gamma_N > 0$ . If  $c_N \to 0$ ,  $Nc_N^4 \to \infty$ , and  $\gamma_N \le N^{-3/d} (7 \ln N)^{-1}$ , then there exists a constant  $\alpha > 0$  only depending on k and d, such that the excess risk  $\mathcal{E}_N$  of kernel interpolation estimator  $f_N$  satisfies

$$\mathcal{E}_N = O_{\mathbb{P}}\left(N^{-\alpha}\right) \quad as \ N \to \infty.$$

Proof of Theorem 8. Recall the definition of excess risk,

$$\mathcal{E}_N = \mathbb{E}_{x,D_N} \left[ (f_N(x) - f^*(x))^2 \right].$$

By using the Jensen's inequality twice, we have

$$\mathbb{E}_{D_N} \mathbb{E}_x \left[ |f_N(x) - f^*(x)| \right] \leq \mathbb{E}_{D_N} \sqrt{\mathbb{E}_x \left[ (f_N(x) - f^*(x))^2 \right]}$$
$$\leq \sqrt{\mathbb{E}_{D_N} \mathbb{E}_x \left[ (f_N(x) - f^*(x))^2 \right]}$$
$$= \sqrt{\mathcal{E}_N}.$$

Then by Markov's inequality, for any  $\delta \in (0,1)$  and  $x \in \mathbb{S}^d$ ,

$$\mathbb{P}\left(\mathbb{E}_{D_N}\left[|f_N(x) - f^*(x)|\right] \ge \delta^{-1}\sqrt{\mathcal{E}_N}\right) \le \delta.$$

The proof is completed by combining the above result with Proposition 9 or Proposition 10.

## C Neural Kernels and Kernel Regime

For an over-parametrized neural network of any architecture (e.g., multi-layer perceptron (MLP), residual network (ResNet), convolutional neural network (CNN), Transformer) under standard initialization (Xavier or He initialization) or neural tangent parametrization (Jacot et al., 2018), the stochastic gradient descent (SGD) training dynamics of its output  $f: \mathbb{R}^d \to \mathbb{R}$  can be tracked by the kernel gradient descent

$$\partial_t f_t(x) = -\eta \frac{1}{N} \Theta_{\theta_t}(x, X_N) \ell'(f_t(X_N), Y_N),$$

where  $\eta > 0$  is the learning rate,  $\Theta_{\theta_t}(x, x') := \nabla_{\theta_t} f_t(x)^\mathsf{T} \nabla_{\theta_t} f_t(x')$  is the neural tangent kernel (NTK) and  $\ell(\cdot, \cdot)$  is the loss function.

In the large width limit, the NTK converges to a deterministic kernel  $\Theta$  and remains constant during training (Yang, 2020; Yang & Littwin, 2021). For the MSE loss  $\ell(f(x), y) = \frac{1}{2}(f(x) - y)^2$ , the solution of the kernel gradient descent has a closed form

$$f_t(X_N) = e^{-t\eta N^{-1}\Theta(X_N, X_N)} f_0(X_N) + \left(I - e^{-t\eta N^{-1}\Theta(X_N, X_N)}\right) Y_N.$$

So that

$$f_t(x) = f_0(x) + \Theta(x, X_N)\Theta(X_N, X_N)^{-1} \left( I - e^{-t\eta N^{-1}\Theta(X_N, X_N)} \right) (Y_N - f_0(X_N)).$$

If we take  $t \to \infty$  first and scale the initial output  $f_0$  to be sufficiently small, then the network output converges to kernel ridgeless regression in the large width limit (Arora et al., 2019), defined as

$$f_{\infty}(x) = \Theta(x, X_N)\Theta(X_N, X_N)^{-1}Y_N.$$

Moreover, if we train only the last layer and freeze all other layers after initialization, the evolution of the network output is governed by kernel gradient descent with a different kernel,  $\Sigma$ , namely the *neural network Gaussian process* (NNGP) kernel (Neal, 1996; Lee et al., 2018; Matthews et al., 2018). The corresponding kernel gradient descent yields (Lee et al., 2019)

$$f_t(x) = f_0(x) + \Sigma(x, X_N) \Sigma(X_N, X_N)^{-1} \left( I - e^{-t\eta N^{-1} \Sigma(X_N, X_N)} \right) (Y_N - f_0(X_N)).$$

Both the NNGP and NTK kernels of neural networks are dot-product kernels, and indeed any dot-product kernel can be approximated by the NNGP or NTK of some neural network (Simon et al., 2022). Moreover, the neural kernels induced by general activations share the same properties as common kernels (e.g., Laplace kernels) through the norm equivalence of RKHS (Holzmüller & Schölpple, 2025).

#### **D** Additional results

#### D.1 Hallucination Detection Algorithms

In this section, we provide additional details of the experiments described in Section 3. As mentioned earlier, we introduce a deterministic mapping between a surname and its associated attribute, together with a correlation coefficient  $\rho \in [0,1]$  representing the probability that a surname fully determines the attribute. We then examine the probability that the model output exactly matches the attribute specified by this mapping on hallucinated samples (i.e., individuals that do not exist in the training data), in order to evaluate how much the model is influenced by this spurious correlation. Figure 7 shows that when  $\rho$  is large, the model tends to generate outputs consistent with the pre-defined mapping.

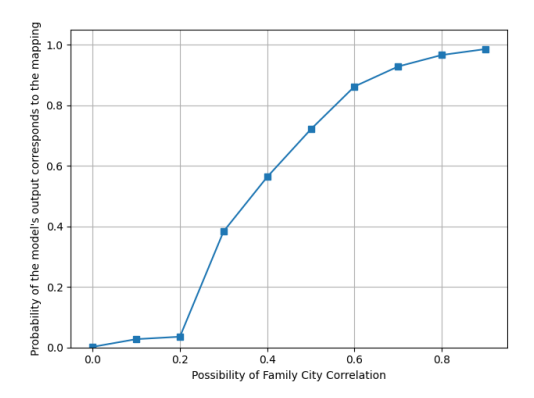
Furthermore, we provide accuracy and TPR@5%FPR of detection methods for experiments in Section 3 (Figures 8 and 9). Across all evaluation metrics (accuracy, TPR@5%FPR, and AUROC in Section 3), performance consistently declines as  $\rho$  increases, suggesting that spurious correlation systematically undermines hallucination detection methods.

We only show the linear probing results for layer 21 as a representative example in the results above; detailed linear probing results of models trained from scratch and models finetuned from SmolLM2-1.7B under each  $\rho$  are provided in Figures 10 and 11.

#### **D.2** Refusal Fine-tuning

In this subsection, we carefully analyze the generalization effect between classes and the third possibility mentioned in the previous discussion. All the following results are completed in a moderated size GPT-2 setting.

The setting here is more detailed, we consider the model fine-tuned after mixing in refusal data that are comprised of 1 to 6 classes of attributes, and evaluate the model on each attribute class separately. For one



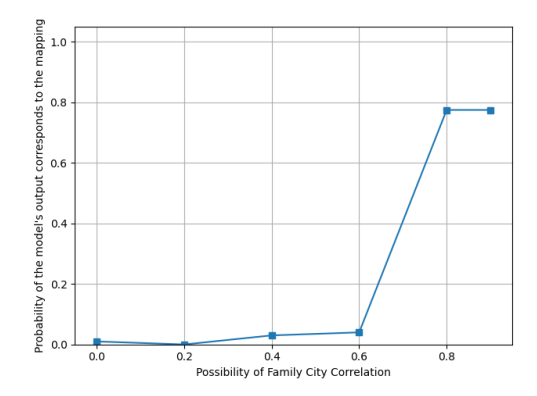
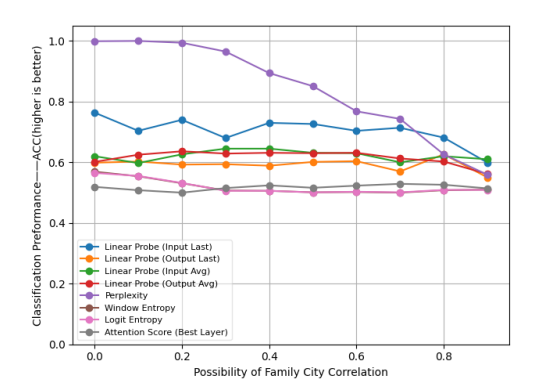


Figure 7: Probability that the model's output corresponds to the predefined deterministic mapping versus  $\rho$ . Left: Experimental results of models learned from scratch. Right: Experimental results of models finetuned from SmolLM2-1.7B. As  $\rho$  increases, the model is more likely to generate outputs that conform to the pre-defined mapping, indicating a stronger reliance on the spurious correlation.



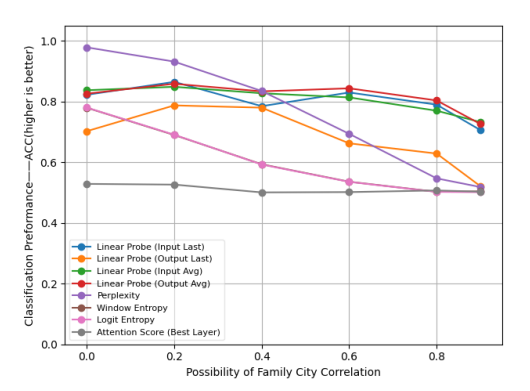


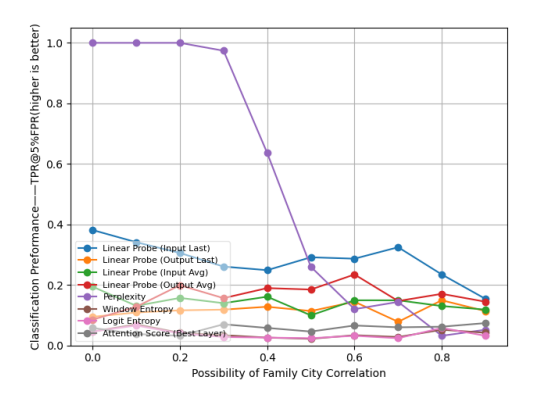
Figure 8: Accuracy of different hallucination detection methods versus  $\rho$ . Left: Experimental results of models learned from scratch. Right: Experimental results of models finetuned from SmolLM2-1.7B.

specific statistics, this procedure generates a  $6 \times 6$  heat maps, displays the generalization ability of training on one subset and evaluating on others.

For example, Figure 12 shows the case of  $\rho=0.0$ . We list 6 tables, each corresponds to an amount under a further fine grained setting. For the left columns, the *same* represents the refusal data is constructed by using same individuals for 6 classes, the right column *different* represents refusal data of 6 classes contain different individuals, we expect the *different* setting has more effect and that is indeed the truth. Then the attribute class caption labeled at the bottom of the heatmap from left to right illustrates the adding order of attributes when the attribute becomes a part of the refusal data. The rows of the heat map from top to bottom corresponds 6 separately fine-tuned model on mixed SFT data when the corresponding number of classes are added into refusal data. For each row, the columns displayed the corresponding metric evaluated on each test data of attribute class. It can be seen that there is no generalization here.

Further more, we add a new hallucination rate metric corresponds the third possiblity mentioned before, it is obtained simultaneously with SFT accuracy, means it is the pure hallucination rate

#{wrong responses on QA pairs of attribute class i}  $\cap$  {not refusal responses} #{QA pairs on attribute class i}



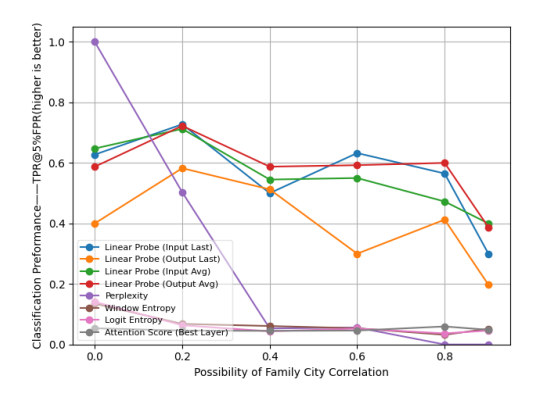


Figure 9: TPR@5%FPR (true positive rate (TPR) when the false positive rate (FPR) is at most 5%) of different hallucination detection methods versus  $\rho$ . Left: Experimental results of models learned from scratch. Right: Experimental results of models finetuned from SmolLM2-1.7B.

on the same test data as in the SFT accuracy heat maps, while refusal rate is tested on another separate data with purely unknown individuals. Notice that each data point discussed in Section 3.2 is of a form as an average of the last row of one heat map under the *same* part.

In Figures 13,14,15 we show the result that varies the correlation from 0.0 to 0.9 and each metric has the same meaning as before.

#### **E** Implementation details

#### **E.1** Dataset Overview

**Basic setting** We uniformly distribute the frequency of each individual's occurrence across all dataset splits, ensuring that each person is represented approximately equally across training, fine-tuning, and testing subsets. Specifically, for our pretraining dataset, we select the first 10,000 individuals and apply 50 templates to each individual; for the instruction fine-tuning dataset, we select the first 5,000 individuals and generate a set of 30 question—answer pairs per individual. The remaining individuals are reserved exclusively for testing purposes to evaluate model performance and hallucination detection.

**Varying the middle name** For the purpose of evaluating the ability of various hallucination detection algorithms, we build a test set using 2,000 individuals from the pretraining dataset. This set includes factual samples based on the original individuals and hallucinated samples generated by altering their middle names to create novel identities absent from training. Using birthplace questions for both groups, detection methods are supposed to classify model outputs as factual or hallucinated without ground-truth access.

**Data for training and testing SmolLM** For continual pre-training, we use a mixture of FineWeb (Penedo et al., 2024) and the pre-training dataset of our synthesized basic setting E.1. To enhance data diversity and improve alignment with natural language, we rewrite our basic synthesized pretraining dataset using Qwen-2.5-3B (Qwen et al., 2025), generating more natural and coherent text representations.

For the instruction fine-tuning dataset, we directly use our synthesized Q&A format applied to the entire 10,000-individual pretraining dataset in the basic setting.

For evaluation, in contrast to the previous setting, we use 2,000 individuals from the instruction fine-tuning dataset as truth samples, and 2,000 random individuals as hallucinated samples (guaranteed not to exist in the training dataset). The test data consist of Q&A questions about their birthplaces.

#### **E.2** Training details

**Basic training detail** For training, we adopt Adam optimizer (Kingma, 2014), use a sequence length of 512 and batch size of 32. We apply a warmup ratio of 0.05 and a warmdown ratio of 0.1. Pretraining runs for 4 epoch with a learning rate of 0.0006, while fine-tuning runs for 1 epochs with a reduced learning rate of 0.0003. We use no weight decay and use bf16 precision. To enhance parallelism, multiple sequences are packed into 512-token sequences, but cross-sequence attention is masked out.

Table 2: Examples of Pretraining and Instruction Fine-Tuning Data

<b>Dataset Type</b>	Example	
Pretraining	"Gracie Tessa Howell is born in Camden, NJ. He studies Biomed-	
	ical Engineering and works at UnitedHealth Group. He enters the	
	world on April 15, 2081, and is employed in Minnetonka. He is	
	an alumnus/alumna of Buena Vista College."	
Instruction Fine-Tuning	"Q: What area of study did Gracie Tessa Howell focus on? A:	
	Biomedical Engineering"	
Refusal Fine-Tuning	"Q: What academic discipline did Daniela Yasmin Marshall focus	
	on? A: I don't know."	

Table 3: Model Configurations with Parameter Counts

Layers	Heads	Emb Dim	Params (M)
4	3	192	11.4
5	4	256	16.8
6	5	320	23.5
7	6	384	31.7
8	7	448	41.8
8	8	512	50.9
9	9	576	64.8
10	10	640	81.3
11	11	704	100.8
12	12	768	123.6
16	16	1024	252.8
20	16	1024	303.2
24	20	1440	669.6
32	25	1600	1063.5

#### E.3 Prompts

This section details the prompts we use for entity extraction and consistency clustering tasks.

Entity Extraction Prompt We use the following prompt to instruct the model to extract all possible entities from a given question, preserving their exact text and character offsets.

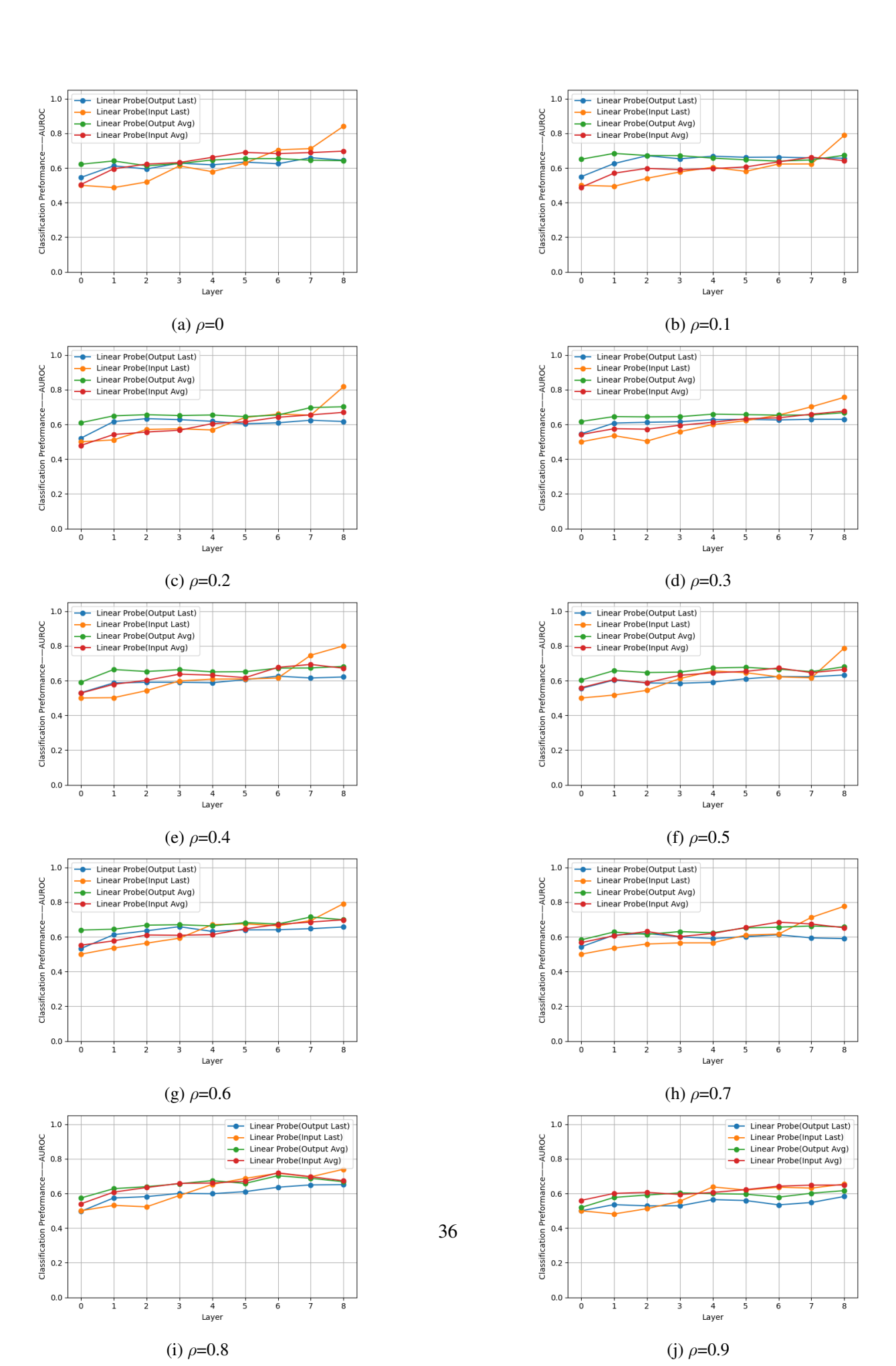
```
Entity Extraction Prompt (QUESTION PROMPT)
Task: From QUESTION, extract ALL possible entities (people, orgs, works,
   locations, events, dates, numbers, titles, etc). Include overlapping/
   nested spans (e.g., \textit{University of California} and \textit{
   University of California, Berkeley )).
Rules:
- Return unique items but keep overlaps as separate entries.
- Preserve the exact surface text and its character start/end offsets.
- Add a coarse type: ["PERSON", "ORG", "WORK", "LOC", "EVENT", "DATE", "NUM", "
   TITLE", "OTHER"].
- Do NOT infer beyond the question's text; no web lookup.
- If uncertain, include as OTHER.
- Keep it terse.
Output ONLY valid JSON:
{ {
  "question": "{{will be filled}}",
  "entities": [
      "text": "surface form",
      "start": <int>, // char index
      "end": <int>,
                      // exclusive
      "type": "PERSON|ORG|WORK|LOC|EVENT|DATE|NUM|TITLE|OTHER"
    } }
  1
} }
Input:
QUESTION: {question}
```

**Consistency Clustering Prompt** To evaluate the consistency of model predictions, we use the following prompt to cluster semantically equivalent answers and compare them against a gold label.

```
Consistency Clustering Prompt (CONSISTENCE PROMPT)

Task: Given a QUESTION, a gold LABEL, and 10 PREDICTIONS (prediction_0... prediction_9), cluster PREDICTIONS by semantic equivalence (same core answer). For each cluster, set a short canonical **entity name only ** (no sentences) so it can match LABEL cleanly. Also judge whether the cluster matches LABEL (substantive equivalence; wording may
```

```
differ).
Rules:
- Canonical MUST be just the entity name (e.g., \textit{Michio Sugeno}, \
   textit{October 2010}) -- no verbs, no extras.
- Ignore casing, punctuation, formatting, honorifics, and minor phrasing.
- Numbers/dates must agree (same value or clearly equivalent).
- Empty/unknown/irrelevant predictions -> their own cluster, not matching
    LABEL.
- Keep reasons brief.
Output ONLY valid JSON with these fields:
  "question": "{{will be filled}}",
  "label": "{{will be filled}}",
  "clusters": [
    { {
      "canonical": "short canonical phrasing of this cluster's meaning",
      "count": <int>,
      "members": [<int indices of predictions in this cluster>],
      "matches_label": true|false,
    } }
 ],
} }
Inputs:
QUESTION: {question}
LABEL: {label}
PREDICTIONS:
0: {prediction_0}
1: {prediction_1}
2: {prediction_2}
3: {prediction_3}
4: {prediction_4}
5: {prediction_5}
6: {prediction_6}
7: {prediction_7}
8: {prediction_8}
9: {prediction_9}
```



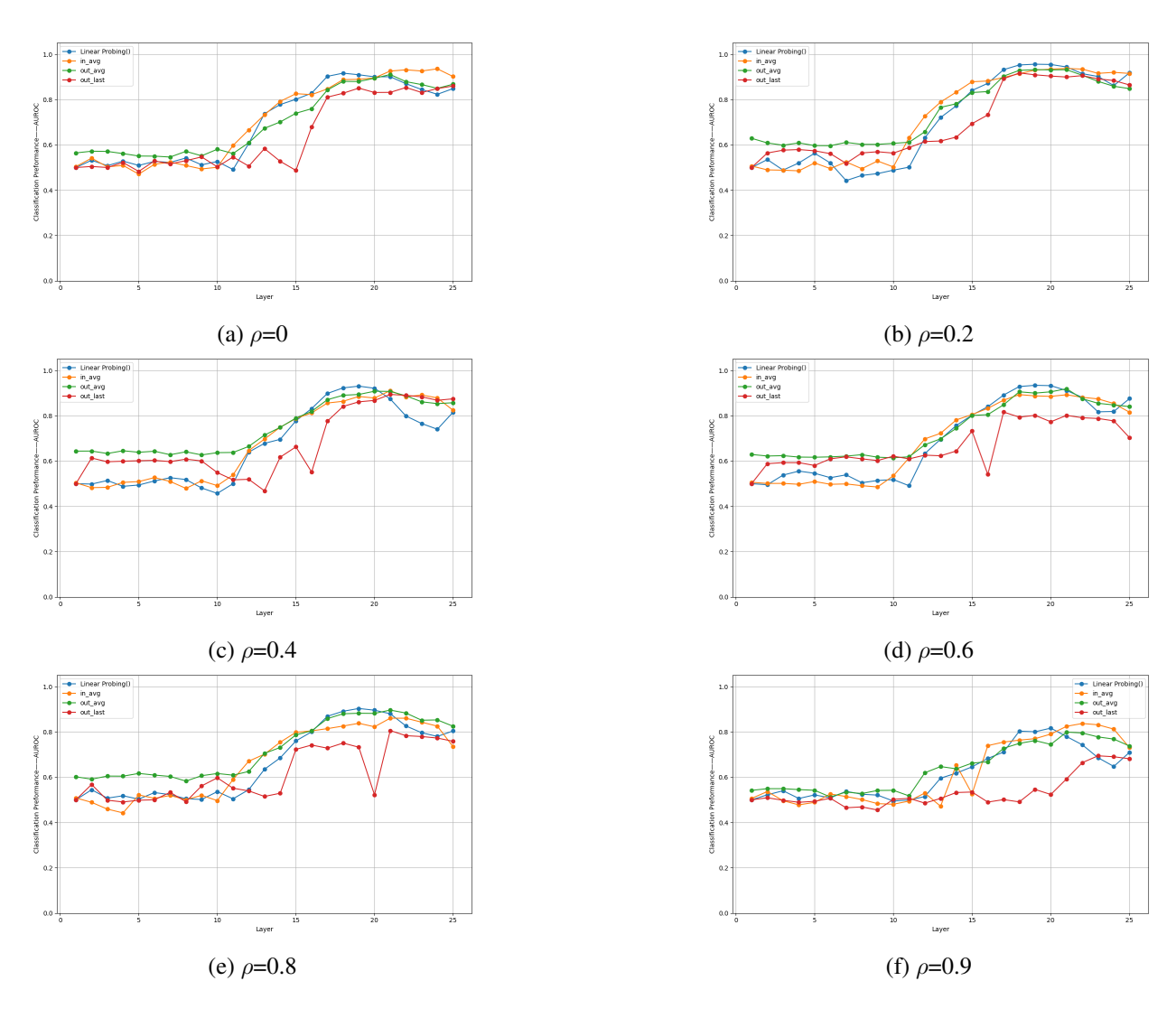


Figure 11: Linear probing results for different  $\rho$  settings of model continual-pretraining and SFT from SmolLM2-1.7B. Each subfigure shows the probing performance(AUROC) of single  $\rho$ .

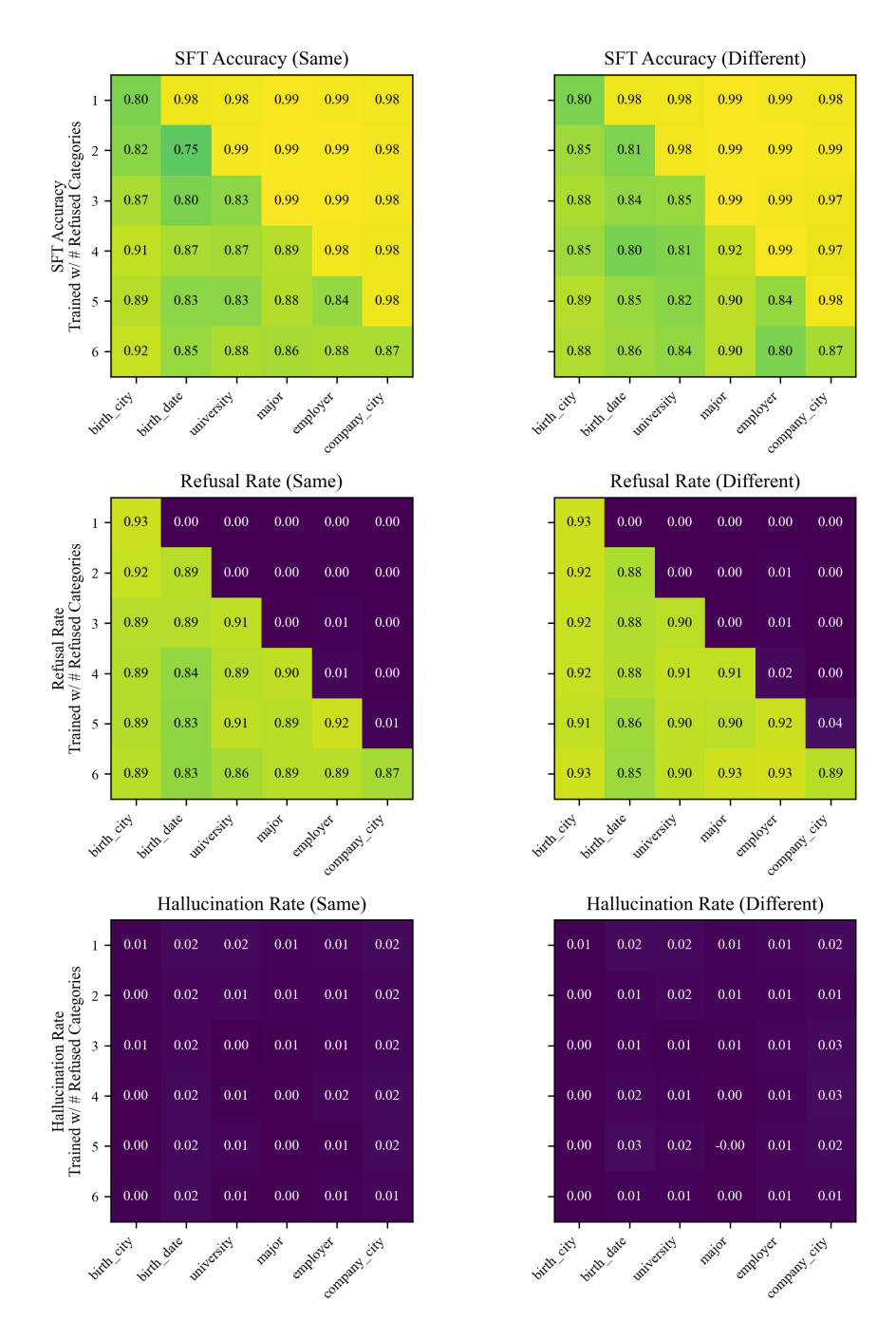


Figure 12: Example of detailed experiment under class-alone level testing. The left part shows the result tested on providing same individuals to each refusal data, the right part distribute different individuals to the refusal data of each class. We make this distinction here to study the effect of the difference in capacity occupancy caused by different names( use different people to construct data of different classes will occupy more parameter capacity). From top to the bottom are the result of accuracy value, refusal rate, hallucination respectively. We found here the generalization effect is minimal and there almost correct answer or *I don't know*. during testing on known individuals.

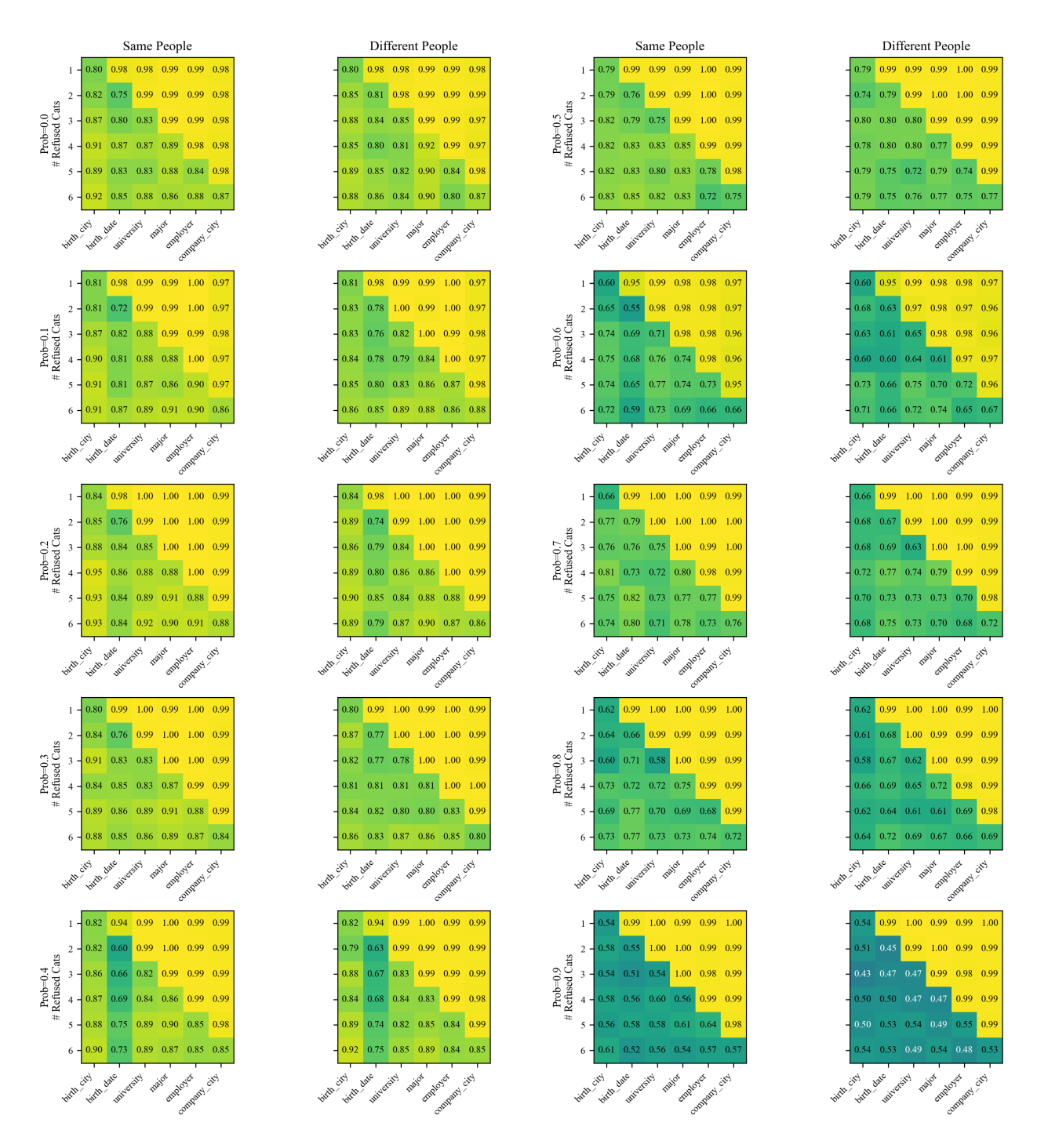


Figure 13: Results of accuracy with correlation intensity from 0.0 to 0.9. High correlation level heavily damage the accuracy, and training on some subset of attributes does not harm the others.

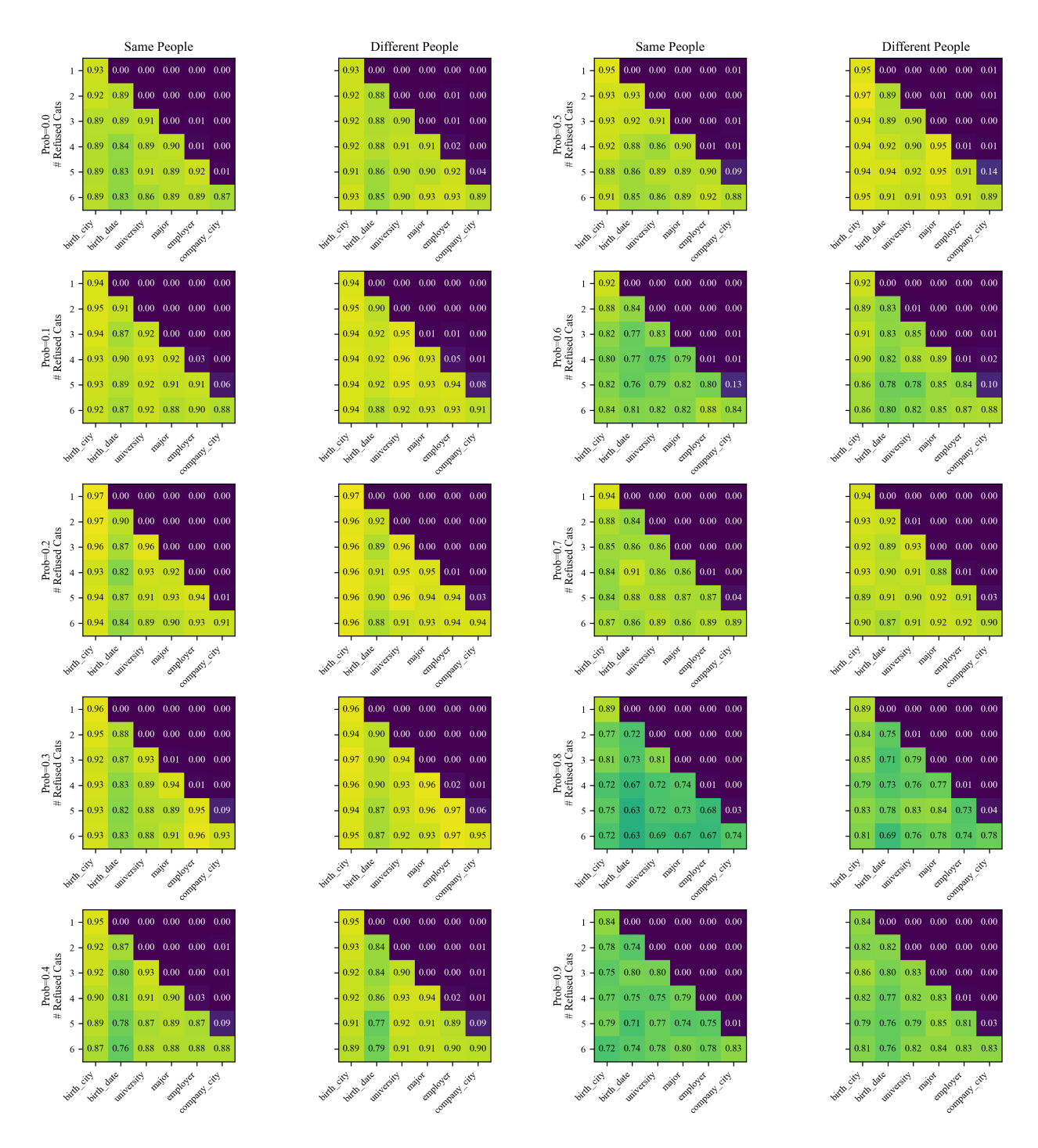


Figure 14: Results of refusal rate with correlation intensity from 0.0 to 0.9. High correlation also causes a decline in refusal rate, and training on some subset of attributes does not contribute to the others. In each heat map, the performance of first row is better than the last row, this is due to our fixed volume data mixing scheme that maintains the refusal data proportion at 12%. More classes share a fixed total amount, this results in a reduced amount of data allocated to each class.

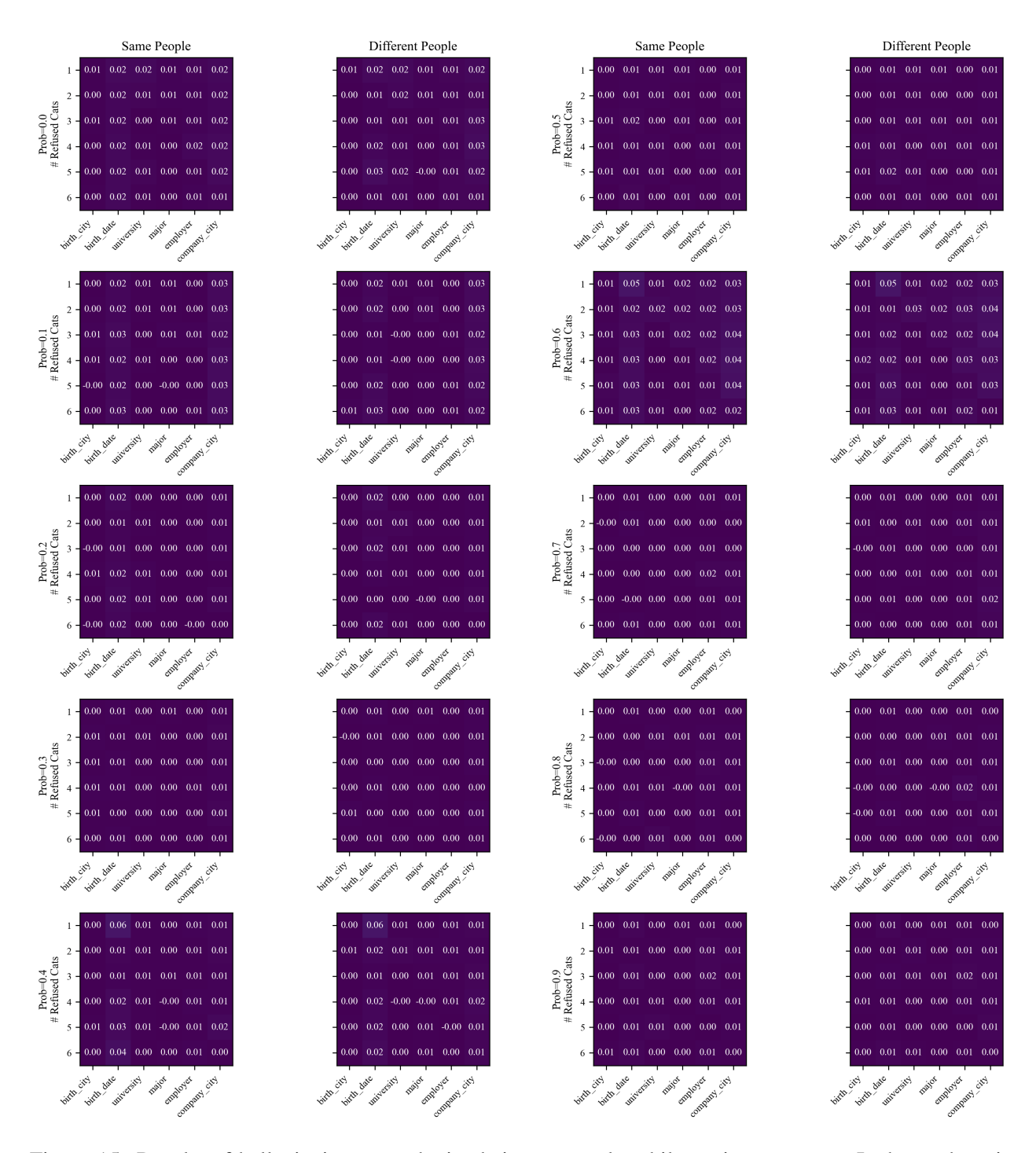


Figure 15: Results of hallucinaion rate, obtained simutaneously while testing accuracy. It shows there is almost no hallucination occurs when evaluating at known individuals. The deteriorated accuracy almost stem from over-refusal.